



FCTUC FACULDADE DE CIÊNCIAS
E TECNOLOGIA
UNIVERSIDADE DE COIMBRA
DEPARTAMENTO DE
ENGENHARIA MECÂNICA

Tribological study of TMD coatings for rubber applications

Submitted in Partial Fulfilment of the Requirements for the Degree of Master in Materials Engineering

Author

Geet Raju

Advisors

Albano Cavaleiro

Evaristo Peralta

Jury

President	Professor Doutor Bruno Trindade Professor Associado da Universidade de Coimbra
Vowels	Professor Doutor Mitjan Kalin Full Professor at University of Ljubljana Doutor Ana Manaia Coordenadora de Projectos, IPN LED&MAT
Advisor	Professor Doutor Albano Cavaleiro Professor Catedrático da Universidade de Coimbra

In the framework of Joint European Master in tribology of Surfaces and Interfaces



Coimbra, July, 2015

LIST OF CONTENTS

LIST OF FIGURES.....	III
LIST OF TABLES.....	V
ACKNOWLEDGEMENT.....	VI
RESUMO.....	VII
ABSTRACT.....	VIII
1. INTRODUCTION.....	1
1.1 INDUSTRIAL PROBLEM.....	1
1.2 FRAMEWORK.....	2
1.3 TRANSITION METAL DICHALCOGENIDES (TMD) COATINGS.....	2
1.3.1 Structure and Properties.....	2
1.4 TRIBOLOGY.....	4
1.4.1 Concepts.....	4
1.4.2 Coatings.....	5
1.5 CHARACTERISATION AND EVALUATION.....	6
1.5.1 Microscopy.....	6
1.5.2 Scanning Electron Microscopy (SEM).....	6
1.5.3 X-Ray Diffraction (XRD).....	6
1.5.4 Nanoindentation.....	7
1.5.5 Tribological Evaluation.....	8
1.6 ACRYLONITRILE BUTADIENE RUBBER (NBR).....	9
1.6.1 Properties.....	9
1.6.2 Structure.....	10
2. STATE OF THE ART.....	11
2.1 PROPERTIES AND DRAWBACKS OF TMD FILMS.....	11
2.2 DOPING OF TMD FILMS.....	12
2.3 DEPOSITION METHODS FOR W-S-C FILMS.....	16
2.3.1 Magnetron Sputtering.....	17
2.3.2 Reactive Magnetron Sputtering.....	18
2.4 PERFORMANCE OF TMD-C FILMS.....	19
2.5 TRIBOLOGICAL BEHAVIOUR OF NBR.....	20
3. METHODOLOGY.....	21
3.1 MATERIALS.....	21
3.2 CHARACTERIZATION METHODS.....	21
3.2.1 Adhesion Test.....	21
3.2.2 X-Ray Diffraction.....	22
3.2.3 Scanning Electron Microscopy.....	23
3.2.4 Nanoindentation.....	23
3.2.5 Ball-on-Disk.....	23
3.2.6 Optical Microscopy.....	24
4. RESULTS.....	25
4.1 STRUCTURAL CHARACTERISATION.....	26
4.2 TRIBOLOGICAL PERFORMANCE.....	29
5. CONCLUSION.....	43
6. REFERENCES.....	44
7. APPENDIX.....	51

LIST OF FIGURES

Figure 1 - Structure of WS₂, in 2D and 3D view (left and middle), and turbostratically stacked WS₂ in 3D view (right). W atoms = dark grey, S atoms = light grey, c axis = vertical line in the paper. [2]..... 3

Figure 2 - Schematic picture showing the normal (F_N) and friction (F_F) forces on a sliding object [2]..... 4

Figure 3 - Information depth (above) and scanning process (below) for different XRD setups. [2] 7

Figure 4 - Schematic load-displacement curves [2] 8

Figure 5 - Ball-on-disc setups with rotating geometry [2] 9

Figure 6 - Structure of NBR [11]..... 10

Figure 7 - Scanning electron micrographs of a porous, crystalline type I W-S coating in cross-section view (left) and top-view (right) [12]..... 11

Figure 8 - W-S-C films designs: A) Nanocomposite coatings with hard WC nanoparticles embedded together with WS₂ nanograins in an amorphous carbon matrix); B) nanograins of WS₂ in a C-matrix; C) film with super-lattice WS₂ + C layers [6]..... 14

Figure 9 - A magnetron sputtering system during co-sputtering from two targets [2].. 18

Figure 10 - Raman spectra taken from the center of the wear track as a function of the test duration (a) and applied load (b) [6]. 20

Figure 11 - The scratch test equipment used for adhesion tests. 22

Figure 12 - The XRD setup used for this work. 22

Figure 13 - The SEM instrument at IPN, LED & MAT used for studying the structure and the wear tracks of the coatings..... 23

Figure 14 - The home-made pin-on-disk test rig used for studying the tribological behaviour of the coatings against rubber. The setup of the heating apparatus was done in a way to maintain the substrate surface temperature as close to the desired temperature as possible. The maximum temperature used for these tests was 200 °C..... 24

Figure 15 - The optical microscope used in the current work. 24

Figure 16 - Carbon content plotted against power ratio. 26

Figure 17 - SEM images of the crystalline pure W-S coating in its cross-section view (left) and top-view (right)..... 27

Figure 18 - XRD diffractograms of W-S-C films as a function of carbon content 28

Figure 19 - Mechanical properties of W-S-C films as a function of C content with respect hardness 29

Figure 20 - Comparison of avg. coefficient of friction for the co-deposited coatings at all temperatures..... 30

Figure 21 - Friction coefficients of the co-deposited coatings at 25⁰C (above). Image of the contact area of the NBR ball taken after the test against pure WS₂ coating showing the presence of a shiny WS₂ tribo-layer on the ball surface (below)..... 31

Figure 22 - Friction coefficients of the co-deposited coatings at 100⁰C (above). Image of the contact area of the NBR ball taken after the test against pure WS₂ coating showing the presence of a shiny WS₂ tribo-layer on the ball surface (below). 32

Figure 23 - Wear track for WSC64 against NBR at 100⁰C as analysed under a microscope (left) and SEM (right). 33

Figure 24 - Friction coefficients of the co-deposited coatings at 200⁰C (above). Image of the contact area of the NBR ball taken after the test against pure WS₂ coating showing the presence of a smooth, shiny WS₂ tribo-layer on the ball surface (below)..... 35

Figure 25 - Comparison of friction: a) friction for 100Cr6 balls at RT and 200C, and friction behaviour of pure WS2 coating for longer and shorter cycles at b) RT and c) 200C	36
Figure 26 - Comparison of friction: a) friction for 100Cr6 balls at RT and 200C, and friction behaviour of WSC49 coating for longer and shorter cycles at b) RT and c) 200C	37
Figure 27 - Images of the 100Cr6 (left) and NBR (right) balls taken after test on WSC49 at 200 ⁰ C with longer cycles.....	38
Figure 28 - Comparison of friction: a) friction for 100Cr6 balls at RT and 200C, and friction behaviour of WSC64 coating for longer and shorter cycles at b) RT and c) 200 ⁰ C	39
Figure 29 - Images of the 100Cr6 (left) and NBR (right) balls taken after test on WSC64 at 200 ⁰ C with longer cycles.....	40
Figure 30 - Friction comparison chart for tests at all temperatures.....	41
Figure 31 - Optical and SEM images of the WSC49 coating at 200 ⁰ C (top) and WSC64 coating at 200 ⁰ C (bottom) for longer cycles.	42

LIST OF TABLES

Table 1 - Properties of NBR [10].....	10
Table 2 - Chemical composition of AISI 316L [73].....	21
Table 3 - Chemical composition and thickness of W-S-C coatings.	25
Table 4 - Mechanical properties of the coatings	29
Table 5 - Comparison of friction and wear rates of the co-deposited coatings at 25 ⁰ C. 31	
Table 6 - Comparison of friction and wear rates of the co-deposited coatings at 100 ⁰ C.	34
Table 7 - Comparison of friction and wear rates of the co-deposited coatings at 200 ⁰ C.	35

Acknowledgement

First and foremost, I would like to thank Prof. Albano Cavaleiro for giving me the opportunity to work in his group. It was one of the most educational experiences of my life. To Dr. Manuel Evaristo, I would like to thank for being there with me every single day from the start to the completion of the project work. My sincere gratitude to Ana Manaia and to Instituto Pedro Nunes (IPN, LED & MAT) for allowing me to do the preliminary tests and later, to perform characterization tests on my test samples.

I would also like to thank Prof. Mitjan Kalin (co-ordinator, TRIBOS program) for considering me to be a part of this wonderful master's program. To Prof. Bruno Trindade, for being patient with us and helping us out with everything here in Coimbra. A big thank you to all the lecturers and PhD. students with whom I have worked with at some point during the past two years.

I would like to thank my family for being the pillar of strength and support that they always are. To all my TRIBOS colleagues, who have shared this wonderful TRIBOS experience with me and have taught me something new and inspired me every single day. Finally, I would like to thank Aysu for sharing all the stressful times over the past year and for making this journey a truly memorable one.

RESUMO

Os revestimentos de Dicalcogenetos de Metais de Transição (DMT) pertencem à classe de materiais com propriedades auto-lubrificantes. Em condições favoráveis podem apresentar coeficientes de atrito extremamente baixos. O uso destes materiais na indústria de moldagem de componentes plásticos pode tornar-se relevante, onde uma das maiores dificuldades é a desmoldagem das peças do molde, o que leva a um aumento das perdas e diminuição da produção. Para o estudo foram depositados três revestimentos do sistema W-S-C para estudar o seu comportamento tribológico em deslizamento contra borracha acrílico-nitrilo butadieno (NBR) como contra corpo. Os revestimentos foram depositados com teores crescentes em carbono 0, 49 e 64 % atômico de carbono. Os revestimentos foram caracterizados em ensaios de pino disco a diferentes temperaturas, temperatura ambiente, 100 e 200 °C. O coeficiente de atrito para o revestimento de WS_x sem carbono apresentou um comportamento idêntico para todas as temperaturas testadas. No entanto, para ambos os revestimentos dopados com carbono à temperatura ambiente e a 100°C apresentaram coeficientes de atrito bastante elevados. Com o aumento da temperatura para 200°C observou-se uma redução acentuada do coeficiente de atrito. Uma vez que os revestimentos apresentaram valores de atrito elevados, os revestimentos foram também testados com um maior número de ciclos e uma carga normal superior. Novamente o revestimento W-S sem carbono foi o que apresentou o melhor desempenho. A composição química, estrutura e morfologia foram analisadas e posteriormente correlacionadas com as propriedades mecânicas. A dopagem dos revestimentos com carbono origina um aumento substancial da dureza para valores de 7-7,5 GPa, sendo o valor máximo obtido para o teor de carbono de 64 % at. Os padrões de difração de raios X mostram que com o aumento do teor em carbono dos revestimentos há uma perda de cristalinidade, com os revestimentos dopados com carbono a apresentarem espectros típicos de estruturas amorfas. As pistas e partículas de desgaste foram analisadas por Microscopia Electrónica de Varrimento para observar possíveis transformações estruturais ocorridas pelo aumento da carga aplicada. Os resultados do coeficiente de atrito foram comparados com os modelos existentes para os DMT puros, tendo-se concluído que os mecanismos de deslizamento para os revestimentos do sistema W-S-C, nas condições testadas, é distinto do comportamento para os revestimentos de DMT puros quando utilizado contra NBR.

Palavras chave: Dicalcogenetos de Metais de Transição, DMT, W-S, NBR

ABSTRACT

Transition metal dichalcogenides (TMDs) are a promising solid, self-lubricating family of thin films. They possess the property of “superlubricity” in favorable conditions. Their use may become relevant in the polymer molding industry, where a lot of material is wasted due to problems of mold release and fouling. Three different W-S based coatings were deposited in order to check their tribological behaviour against acrylonitrile butadiene rubber (NBR) as the counter body. Two of these coatings were alloyed with 49 at.% and 64 at.% of carbon. The deposited samples were then tested with a pin-on-disk test rig at room temperature (RT), 100 °C and 200 °C. The friction coefficient for the pure W-S coating showed a similar behaviour across all temperatures. However, for both the C-alloyed coatings, the friction coefficient obtained was very high for both RT and 100 °C. A marked improvement in friction was only observed at 200 °C for both these coatings. Durability tests for these coatings were also conducted on the pin-on-disk with a longer number of cycles and a higher load. Again, the pure W-S performed better than the C-alloyed coatings. The chemical composition, structure and morphology of the coatings were analyzed and correlated with the mechanical properties. Alloying W-S films with carbon led to a substantial increase in the hardness of the coatings to around 7-7,5 GPa; the maximum hardness was obtained for the coatings with carbon contents close to 64 at.%. XRD diffraction patterns showed that there was a loss of crystallinity with the increase of the carbon content in the film. The wear tracks and wear debris were also analyzed by SEM to understand the structural transformations induced by the increasing load. The friction results were compared with existing models for pure transition metal dichalcogenides (TMD), and it could be concluded that the friction mechanisms of W-S-C coatings fundamentally differ from those of pure TMD when used against NBR.

Keywords: transition metal dichalcogenides, TMD, W-S, W-S-C, NBR

1. Introduction

Sustainable development and how to cope with limited resources of materials and energy has been a major challenge for modern technology. It is just as imperative to think about limiting the use of energy as it is to think about finding novel methods of producing it. The concepts of friction and wear, which largely concerns with the branch of science called tribology, are an ever-present phenomena intimately connected with energy and material loss. It is said that in passenger cars, one-third of the fuel energy is used to overcome friction in the engine, transmission, tires, and brakes [1]. Reduction of friction and wear, therefore, offers the possibilities of saving energy and materials by not only reducing the energy needed for operation but also increasing component lifetimes.

The role of a lubricant is to prevent opposite surfaces from coming into close contact with each other, thereby preventing their mutual destruction. Liquid lubricants have been used to suppress or to limit the contact pressure, to reduce the friction and to facilitate sliding between solid bodies. Further, they allow the reduction of heating generated by friction. In many cases, the presence of liquid is neither possible nor recommended, or it can even be prohibited to avoid the contamination of the product which is in contact with. This is particularly true for vacuum environments, mechanisms where it is necessary to maintain very low tolerances, and applications in materials with incompatibility problems. In the manufacturing industry whenever two solids slide against each other deterrence of liquid lubricants is a great challenge. Examples are the diversity of components in engines, and even more importantly the vast range of materials processing operations like stamping or cutting. Consequently, the design and development of self-lubricating coatings became an attractive subject of applied research.

The question of reducing friction and wear becomes highly relevant in the polymer molding industry where a lot of rubber is wasted due to problems of mold release and fouling. These problems have incurred huge losses to the rubber making industry and any solution in the form of chemical agents is not a permanent and a long lasting one. One way of correcting the situation would be to work on the surface of molds and to use low-friction, low-wear coatings which would not allow material wastage during mold release.

1.1 Industrial Problem

Optimizing a component tribologically by suitable design of its surface is achievable as friction and wear are surface phenomena. One way to achieve this is to apply a coating, an approach which has been used in this work. The thickness of the coating is often only a few micrometers, i.e. a few thousandths of a millimeter, or a few percent of the thickness of a human hair. Still, it can vastly decrease the friction and wear. The focus of this work has been triboactive coatings, which change and adapt [2] when sliding against another surface, leading to the formation of a slightly different material on the outermost part of the coating. This so-called tribofilm is usually only a few tens of nanometers thick [2], but has a significant effect on coating performance.

The polymer molding technology comes with an intrinsic problem of removing the molding from the molds. This is also the main cause of limiting production rates. Another problem which limits production rate, is the build-up of deposits on the mold surface after a certain number of mold cycles depending on the target material used. Problems of mold release and fouling are very common in the polymer processing industry. They result in a serious limitation on the production rate and represent a significant cost to the industry. The large number of commercial release products available from many different manufacturers is in itself evidence that there is no proper solution to this problem as yet.

In this work, sulfide- and/or carbide-based low-friction coatings have been investigated. The aim has been to understand the connection between the composition and the structure of the coatings, how they change in a tribological contact (by the formation of tribofilms) against Buna N Acrylonitrile Butadiene (NBR) counter-body, and the tribological performance in terms of friction and wear. The coatings have thus been studied on the microscopic as well as on the macroscopical scale.

The background of the scientific questions is discussed in the following chapter, as well as the issues addressed in the different papers constituting the basis of this thesis.

1.2 Framework

The project presented in this work is undertaken on behalf of the University of Coimbra in collaboration with Instituto Pedro Nunes (IPN, LED & MAT), Coimbra. The objectives and the goals of the said project are highly relevant to the industry and therefore defined accordingly.

The title of the project is "Tribological study of TMD coatings for rubber applications." The introductory section of this work establishes the nature and the outlines describing the problems faced in the industry and the kind of work undertaken in this project to overcome the same. A detailed description of the current knowledge and advances in the said field is defined in the following section, which entails not only the physical definition of the problem but also existing applications, established paths and gaps in understanding of the phenomenon, followed by the established objectives of the study, the final findings, and all the established protocols, methods and selected materials.

1.3 Transition metal dichalcogenides (TMD) coatings

1.3.1 Structure and Properties

Transition metal dichalcogenides (TMDs) are compounds with the general formula MeX_2 ($Me = W, Mo$; $X = S, Se$). Their layered structure (X-M-X type) is highly anisotropic which is precisely why they have been the scope of many research studies. Every sheet of metal atoms is sandwiched between two layers of chalcogen atoms. A trigonal prism

of chalcogen atoms coordinates each metal atom [3]. The bonds between the metal and the chalcogen atoms are strong and are involved within the sandwich layer whereas, only weak van der Waals interactions are present between the layers. The (001) basal plane surface is only reactive in the presence of defects while the plane edges have dangling bonds [2].

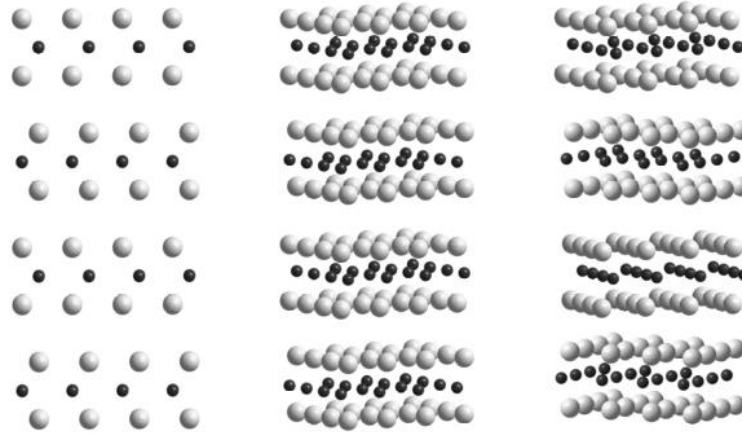


Figure 1 - Structure of WS_2 , in 2D and 3D view (left and middle), and turbostratically stacked WS_2 in 3D view (right). W atoms = dark grey, S atoms = light grey, c axis = vertical line in the paper. [2]

TMDs in their most common form have a stacking sequence of two sandwich layers, giving a hexagonal symmetry, denoted as 2H- MeX_2 . When there is a stacking sequence of three sandwich layers, a lesser-known rhombohedral form 3R- MeX_2 is resulted [3]. It is also possible to have a disordered stacking. The so-called turbostratic stacking (Figure 1) is obtained when the sandwich layers are parallel but more or less randomly rotated around the c axis.

The shear strength parallel to the planes is very low due to the weak bonding between the sandwich layers, and this allows the TMDs to be used as solid lubricants. Much of the work on two of the most commonly used TMDs (MoS_2 and later also on WS_2) has been focused on vacuum or space applications, since the TMDs are known to perform best in these environments. Herein lies an important difference between graphite and TMD lubrication. Graphite lubrication largely requires the presence of intercalating species (such as H_2O) to obtain low friction, while the TMDs perform best in the absence of such contaminations and are intrinsic lubricants [4].

The highly anisotropic crystal structure of TMDs (MoS_2 in this case) has been the cause of observance of “loss” of friction according to Martin et al [5]. The frictional anisotropy of friction-oriented sulfur basal planes of MoS_2 grains is what results in a superlubric state [5]. Such tribological properties can only be observed when, i) there is an absence of contaminants in the TMD material which does not lead to the modification of the crystal lattice, ii) there is a formation of a well-adhered TMD transfer layer on the counterpart resulting in very low friction between the surfaces in contact, and iii) reorientation of the (001) basal planes of the TMD grains [6].

1.4 Tribology

The science of interacting surfaces in relative motion is called tribology. It includes the subjects of friction, wear and lubrication. Tribology, while more often used in case of mechanical engineering, involves many aspects of our daily lives such as walking or riding a bicycle, etc. Minimizing friction and wear has a direct impact lowering energy consumption, improvement of performance and so on. Therefore, tribological optimization is of utmost importance for economic reasons among others.

1.4.1 Concepts

The phenomenon of resistance towards relative movement of surfaces is called friction. This phenomenon is quantified using the term - friction coefficient μ , which is defined as the ratio between the tangential force (F_F) and the normal force (F_N). The resistance to the onset of sliding is called static friction while the friction between two surfaces in relative motion is called dynamic friction.

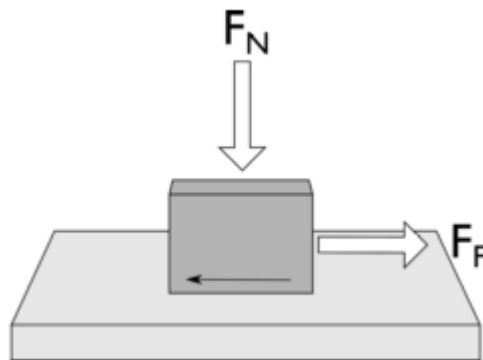


Figure 2 - Schematic picture showing the normal (F_N) and friction (F_F) forces on a sliding object [2]

The friction measured is directly dependent on the material in question and the parameters used during the test for friction measurement affects the measured coefficient of friction.

The removal of material from its original position is called wear. The quantification of wear, in case of sliding contacts, is often in terms of specific wear rate (K'), which is the worn volume divided by the sliding distance (S) and the applied load (F_N):

$$K' = \frac{V}{SF_N}$$

The unit of wear rate is m^2N^{-1} , but usually given as $\text{mm}^3\text{N}^{-1}\text{m}^{-1}$ or $\mu\text{m}^3\text{N}^{-1}\text{m}^{-1}$.

It is generally believed that high friction leads to high wear but such is not necessarily the case as a material such as WS_2 , which is soft and can be easily sheared, has low friction but gives high wear.

The practice of using a lubricant to reduce friction between surfaces is called lubrication. Oils, either base or synthetic containing various additives, are common liquid lubricants. Solid lubricants, however, are materials such as graphite or TMDs. This work entails the use of TMDs used as a coating. The contact surfaces are unlubricated and run against each other in dry conditions. An effect of structural or chemical changes of the materials in contact leads to the formation of tribofilms or tribolayers on surfaces. In order to achieve tribological optimization, the control and understanding of the behaviour of the tribofilms is important.

1.4.2 Coatings

When designing mechanical components, a large number of aspects are taken into consideration, many of which concern mechanical bulk properties and how to avoid for example fatigue, fracture or yielding. Unfortunately, materials that are suitable in these aspects are not necessarily beneficial from a tribological point of view. A common solution to this problem is to modify the surface, so that the materials in the bulk and on the surface are optimized for their respective role. One way of modifying the surface is to apply a coating. Even if the coating only has a thickness of a few μm (i.e. only a few percent of the diameter of a human hair), it can drastically change the properties of the surface. An example of great importance in Swedish industry is the deposition of hard, wear-resistant coatings onto cemented carbide cutting tools. In this work, the main interest is low-friction coatings, with a sufficient wear resistance. The terms coating and (thin) film can be used interchangeably, but coating is favored in this text, in order to avoid confusion with tribofilms.

On closer inspection, it is also possible to distinguish between the bulk and surface properties of the coating, as described in Figure 6. A hard surface can decrease the friction by decreasing the area of the contact spots and the ploughing of asperities. However, to minimize the friction, the shear strength in the interface should be low, which is often found for soft materials. A hard surface with good load-bearing capacity and a very thin layer of a soft, easily-sheared material is a promising solution. The low-friction material can be a tribofilm, which can even be in the nm range and still give low friction. This concept is used for example in carbon-based coatings, where lubricating graphite is formed as a tribofilm on top of a hard and wear-resistant coating. A similar concept with the formation of WS_2 tribofilms is used in this work.

As previously mentioned, the local situation in a tribological contact is often extreme, and the probability for changes of the materials is high. Coatings that spontaneously form and maintain tribofilms with desirable properties, can be defined as triboactive. This means that they change and form beneficial tribofilms by for example chemical reactions, material transfer or structural rearrangements, and preferably do so throughout the lifetime of the component so that the tribofilm is maintained. This approach has been used in the current work, mainly by designing nanocomposite or amorphous coatings from which low-friction WS_2 tribofilms are formed in a tribological contact.

1.5 Characterisation and Evaluation

The current work aims at understanding the composition and structure of the coating material and its effect on tribological behaviour. The coatings were therefore analyzed and characterized before and after testing.

1.5.1 Microscopy

Light optical microscopy was used to study the width of the wear track and the radius of contact of the pin on the disc for the tribometer tests. Electron microscopy, on the other hand, was used to study the coatings in much more detail as their thickness is about 1-2 μm and are therefore too small to be observed under an optical microscope. Electron microscopy uses electrons instead of visible light and thereby has better resolution as the wavelength of electrons are several magnitudes smaller than that of light.

1.5.2 Scanning Electron Microscopy (SEM)

In SEM, an electron beam is emitted from an electron gun and focused on the sample by magnetic lenses. The electrons interact with the atoms of the sample surface, producing a variety of signals which can provide information of the topography and/or composition of the surface. An image is produced by scanning the focused beam over the surface.

A common imaging mode is to detect secondary electrons, which are ejected from the surface when the incoming electrons are inelastically scattered by the atoms of the sample. Secondary electron detection thus gives topographical contrast. It is also possible to detect the electrons from the beam after their interactions with the surface, i.e. back-scattered electrons. Backscattered electron detection thus gives atomic number contrast.

1.5.3 X-Ray Diffraction (XRD)

X-Ray diffraction works on the principle that when a parallel beam of monochromatic X-rays irradiate a sample, it gets diffracted to specific angles due to the sample's atomic lattice which acts as a three-dimensional diffraction grating. The resulting diffraction pattern helps in gathering information about the sample. The most common X-rays used for XRD is the Cu $K\alpha$ radiation with a wavelength of 1.5406 Å. The interactions with the electrons of atoms in a material causes these X-rays to diffract. Crystalline materials have a long range order and when the lattice plane matches a whole number of wavelengths, then positive interference takes place. This is better explained through Bragg's law, which describes the relation between inter-planar spacing d , the wavelength λ and the angle θ between the incident X-rays and the planes [7].

$$n\lambda = 2d \sin\theta$$

The grains in coatings are usually elongated in some direction. Another cause for concern is that crystallite sizes are distributed for most samples but the measurement will only

give an average in the analyzed volume. Strain in the sample can also affect the peaks shapes and position. A Williamson-Hall plot is used to separate the two parameters (crystallite size and strain), both of which can have an effect on the peak width [8]. If the coating is anisotropic, however, or if there is a variation of strain throughout the coating, then such plots are of little use.

The $\theta - 2\theta$ mode is the standard XRD measurement. This mode measures only the reflections from the lattice planes parallel to the surface. As coatings usually do not contain grains with random orientations, unlike powders, so all reflections may not be observed. X-ray measurement of thin coatings involves the use of a mode called the grazing incidence XRD (GI-XRD) to increase the signals from the coatings by the keeping a small and constant incidence angle (1° - 3°) while only scanning the detector (Figure 3).

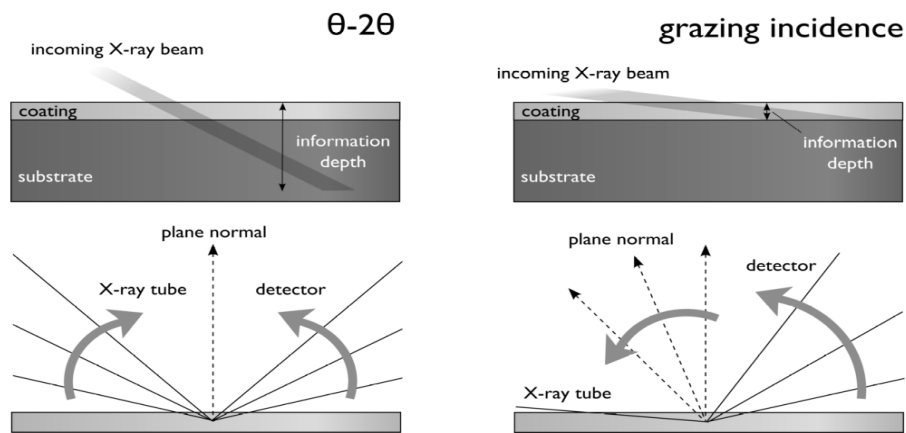


Figure 3 - Information depth (above) and scanning process (below) for different XRD setups. [2]

All the coatings used in this work possess limited crystallinity while a few are even X-ray amorphous. The diffractogram features only broad lumps at low angles as there is no long-range order.

1.5.4 Nanoindentation

Nanoindentation is used to measure the hardness of a small volume of a material. The relation between the applied load and the penetration when a hard tip is pressed into a sample is its measure of hardness. Nanoindentation records the depth of penetration during the indentation process. It is usually performed using a Berkovich tip (a three-sided diamond pyramid with a half angle of 65.35°). A typical nanoindentation test is displayed as a load-displacement curve (Figure 4).

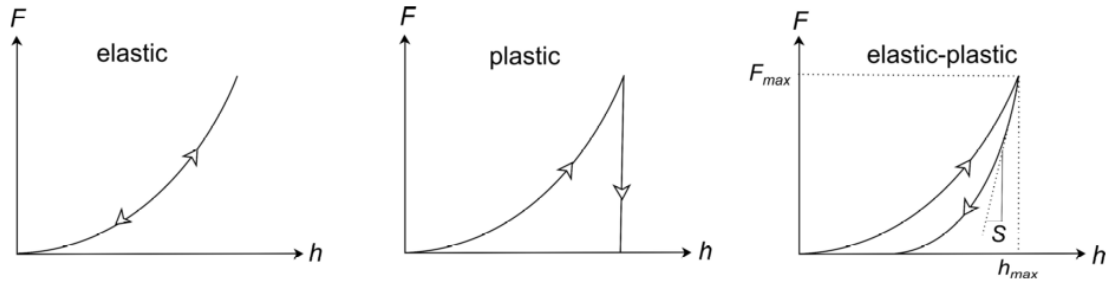


Figure 4 - Schematic load-displacement curves [2]

Most materials are deformed both elastically and plastically. In such a case, the elastic and plastic deformation is displayed by the loading curve whereas, the elastic recovery is displayed by the unloading curve. Measured hardness is calculated from the maximum applied force (F_{max}), and the projected area (A_p):

$$H = \frac{F_{max}}{A_p}$$

The slope of the unloading curve gives information about the stiffness of a material. If the Poisson's ratio of the material is known, then its Young's (or elastic) modulus can be calculated using the Oliver and Pharr method [9]. The measured hardness is dependent on the method used as different methods give different results. The indentation depth is not too deep to avoid substrate effects (with maximum indentation depth at 10% of the coating thickness followed as a rule of thumb).

1.5.5 Tribological Evaluation

Replicating a setting as real as possible can be best used to study the behaviour of a material in its desired application. This, however, is an expensive and a complicated proposition and therefore the use of model setups, which not only allows the study of fundamental aspects but also offers control of parameters so that each effect can be studied, is justified. This work involves the use of a ball-on-disc test rig so that the coating, deposited on a flat substrate, is run against a ball-shaped counter-surface. The ball-on-disc setup has a rotating geometry (Figure 5). The coated sample is attached to a moving sample table whereas the ball, that also has a normal load F_N applied to it, is attached to a stationary pin that is positioned on top of the coated sample. The sample then rotates to create a circular wear track. The ball experiences a friction force F_F , during sliding, measured by a load cell and the coefficient of friction is then calculated as the ratio between F_F and F_N . This setup promotes the possibility of varying the test parameters as well as controlling the atmosphere by using a hood to cover it.

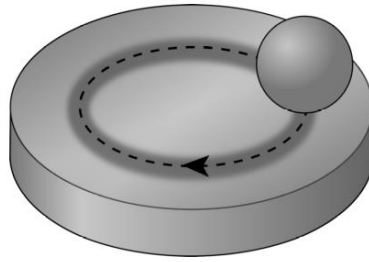


Figure 5 - Ball-on-disc setups with rotating geometry [2]

The coefficient of friction is simultaneously measured during the test while the wear is estimated from analyzing the wear track after the test is run. A cross-sectional area of the tracks is obtained using a laser profilometer, from which the worn volume is calculated. This, in turn, is used to calculate the specific wear rate.

1.6 Acrylonitrile Butadiene Rubber (NBR)

Acrylonitrile butadiene rubbers (NBRs) are widely used for lip seals and ball bearings. NBR has its utility in automotive and mechanical engineering due to its specific thermo-mechanical or tribological properties in the presence of lubricants. NBR chemical formulations can be varied and any modification leads to different mechanical and viscoelastic properties [10]. Any change in the acrylonitrile (ACN) content in the copolymer leads to a change in the viscoelastic properties of the rubber [10]. Simply put, the ACN content makes the rubber matrix less hydrophilic and more polar [10]. This has a direct effect on the glass transition temperature of the rubber which is known to increase with the ACN content which, in turn, influences both rubbery properties and solvent resistance [10].

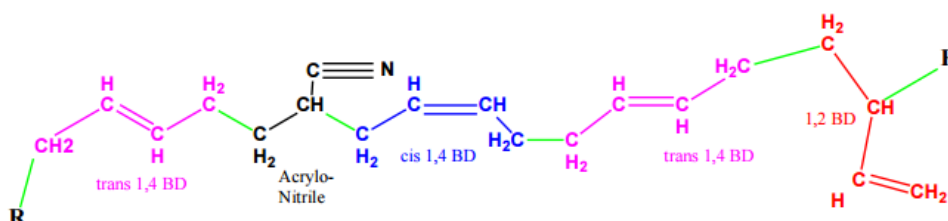
1.6.1 Properties

Amorphous polymers or elastomers form a compound on being treated with various ingredients which in turn, is “vulcanized” to produce rubber. They can return to their original shape without permanent deformation even after being stretched to several times their length. Among other properties of these materials is the one to dissipate energy because of their viscoelastic nature. They are also tough under static or dynamic stress, have an abrasion resistance higher than steel, impermeability to air and water and a high resistance to attack by chemicals or to swelling in solvents [11]. One such elastomer is the acrylonitrile butadiene rubber (NBR) (Table 1).

Table 1 - Properties of NBR [11]

Chemical Name	Common Name	Abbreviation	Properties
Acrylonitrile-butadiene copolymer	Nitrile	NBR	Resistant to water, fuel or other petroleum products. Superior to most elastomers in compression set, cold flow and abrasion resistance. Poor resistance to ozone, sunlight or weather.

1.6.2 Structure

**Figure 6 - Structure of NBR [12].**

An emulsion polymerization system is used to produce NBR. The producers vary the polymerization temperature to make “hot” or “cold” polymers. Acrylonitrile (ACN) and butadiene (BD) can be varied depending on the specific requirements such as oil and fuel resistance or low temperature usages. Each specific NBR grade is defined by two criteria. Primarily, the ACN content determines several basic properties including oil resistance, glass transition temperature and abrasion resistance. A higher ACN content improves all the aforementioned properties. Mooney viscosity is the second criteria used to define a specific NBR grade. Mooney viscosity data of polymers relates to their processing. Materials with a lower Mooney viscosity (30 to 50) are used in injection molding, while those with a higher Mooney viscosity (60 to 80) are used in extrusion and compression molding.

2. State of the Art

Transition metal dichalcogenides (TMDs), in the last three decades, have been widely used as self-lubricating materials. More extensive research has been done on molybdenum disulfide (MoS_2) however, the focus is now shifting to tungsten disulfide (WS_2) due to its improved oxidation resistance and thermal stability withstanding temperatures of about 50– 100 °C higher than the former [13]. It is further claimed that tungsten oxide (WO_3) is not only more protective but it also provides a lower friction coefficient than molybdenum oxide (MoO_3) (0.2–0.3 vs. 0.5–0.6, respectively) [14].

2.1 Properties and Drawbacks of TMD films

Transition metal dichalcogenides or TMDs are used as oil additives or coatings in order to reduce friction. In case of using TMDs as coatings, they could be prepared as thick films (films prepared by electrochemical processes [15], etc.) or thin films deposited mainly by physical vapour deposition (PVD) [16]. Tribochemical reactions during the sliding process on surfaces can also lead to the formation of TMDs [6]. There have also been recent reports on fullerene-like TMDs [17,18] and TMD nanotubes [19,20], with the industrial use of either still being limited, in spite of several successful laboratory tests.

Pure TMD coatings, such as W-S or Mo-S, can be sputtered either from a compound target (non-reactive sputtering) or from a metallic target and hydrogen sulfide gas (reactive sputtering). The resulting coatings are often referred to as MeS_x ($x < 2$) as they are often stoichiometric in sulfur [21]. The coatings may be amorphous or nanocrystalline [21]. Crystalline coatings are often divided according to the orientation of their basal planes. Type I orientation has the basal planes perpendicular to the surface whereas, for type II orientation the basal planes are parallel to the surface [22]. Type I (Figure 1) orientation results in coatings that are highly porous and have loosely packed standing flakes. They have a matte appearance and are black in color. Type II coatings have found favor in being regarded as beneficial for tribological and electrical applications [23].

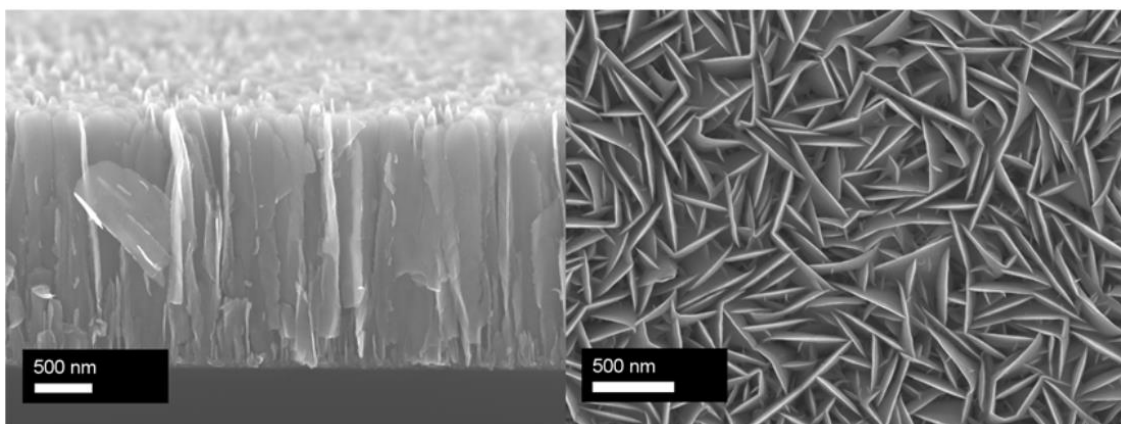


Figure 7 - Scanning electron micrographs of a porous, crystalline type I W-S coating in cross-section view (left) and top-view (right) [12]

TMDs possess the property of superlubricity, which is described as the phenomenon of materials with friction values lower than 0.01. TMDs with their unique, highly anisotropic crystal structure, could behave as superlubricants in the solid state in favorable conditions [6]. According to Le Mogne et al [5], the superlubricity of the MoS₂ film deposited and tested in UHV conditions resulted in friction coefficient values as low as 0.001. This behaviour confirmed the theoretical prediction of the presence of a superlubric state of friction-oriented sulphur basal planes of MoS₂ grains [5,6]. Such tribological properties can only be observed when, i) there is an absence of contaminants in the TMD material which does not lead to the modification of the crystal lattice, ii) there is a formation of a well-adhered TMD transfer layer on the counterpart resulting in very low friction between the surfaces in contact, and iii) reorientation of the (0001) basal planes of the TMD grains [6].

TMD films however, have limitations that need addressing in order to harness their potential. The use of pure TMD films deposited by conventional magnetron sputtering in room conditions is difficult as their deposition by magnetron sputtering unavoidably leads to a disordered structure. Only for a very thin film not exceeding tens of nanometers, can low-friction prominent orientation, (0002), be achieved [16]. TMD films are also known to produce metal oxides when sliding in air and are extremely sensitive to environmental attacks. An increase in friction is due to the presence of WO_{3-x} and MO_{3-x} oxides [24–26]. The {0002} Van der Waals basal plane is more inert to environmental attack than the reactive {1120} plane [27]. Well oriented TMDs with basal planes parallel to surface, therefore, resist oxidation [6]. Storing TMD films in open environment is also known to have detrimental effects on its tribological properties as TMD films, owing to their columnar morphology, are extremely porous and oxygen, water and other reactive species can easily penetrate the film [6]. TMD films have very low hardness when compared with competitive low-friction coatings, such as diamond-like carbon (DLC), typically ranging from 0.3 to 2 GPa depending on stoichiometry, morphology, and deposition conditions [6]. TMD films also do not adhere to steel substrates adequately but a thin metallic interlayer, typically, Ti or Cr results in better adhesion between the film and the substrate [6]. Studies have shown that diselenides are more resistant to water and oxygen attacks. They, however, are not environmentally friendly and so their use is highly limited [16,28]. High contact pressures result in peeling-off of TMD films from substrates, a feature attributed to the low load-bearing capacity of these films which is a direct result of their morphology and low adhesion [6]. Yet another drawback, in many applications, could be the material transfer to the counter-body [6].

Among the various countermeasures applied to remedy the aforementioned limitations are, reduction of water in residual chamber atmosphere to diminish the oxygen content in the film [22], variation of deposition temperature [29] or gas pressure [21,29] and other approaches which have slightly improved the TMD tribological behavior. However, the major issues have persisted and pure sputtered TMD films are restricted to vacuum applications [6].

2.2 Doping of TMD Films

TMD films were doped in order to address some of the issues mentioned earlier such as, increase of density and consequent reduction of porosity, improved adhesion and increase of hardness. The aims, in general, have been achieved. The most successful dopant from

a commercial point of view was titanium (MOST by Teer, Ltd., i.e. MoS₂ doped by Ti), among the many metal dopants (Ti [26,30–33], Al [34], Au [35], Pb [36,37], Ni [35], Cr [38,39]) used in TMD films. There was an evident increase in wear resistance and load-bearing capacity of films, however, now low friction could not be observed [30]. New results, however, do not support such hypothesis [26]. Similar sliding properties were observed upon doping with "inert" metals such Au [6]. The 90s brought about the analysis of non-metallic elements and compounds, such as ZnO [40], Sb₂O₃ [28] and PbO [43]. It must be noted here that there was negligible benefit of doping with these compounds. Every TMD film shows the prevalence of the TMD phase (maximum dopant content is about 20 at. %) and limited interaction between TMD phase and dopants or between TMD elements and dopants. Contamination from residual atmosphere during the sputtering process is not considered as doping.

In order to improve the mechanical properties of the pure TMD coatings, they have been co-deposited with materials known to have better mechanical properties. However, it was soon realized that metals not only have poor friction properties but they are also prone to oxidation. Adding a non-metallic element, then, seemed a viable and a promising alternative and elements such as carbon (C) and nitrogen (N) have been co-deposited with TMDs. The tendency of oxide formation of these elements is a non-issue as their oxides are gaseous and escape the contact without affecting the TMD coating [2]. When TMD coatings are alloyed with non-metallic elements, there is always a possibility that the doping elements might react either with transition metals or dichalcogenides and therefore these coatings have usually shown a higher non-TMD content. A typical example is nitrogen forming tungsten nitride [13,44], niobium forming NbS₂ [45,46], or carbon producing tungsten carbides [13,44,47–50].

Several scientific groups began research on the new concept of coatings based on the alloying of transition metal dichalcogenides (TMDs) with carbon, in the late-90s [6]. Their aim, originally, was to combine the excellent frictional behavior of TMDs in vacuum and dry air with the tribological properties of diamond-like carbon (DLC) coatings [6]. Along with the aforementioned changes, an increase in the coatings compactness in relation to TMDs and an improvement of the mechanical properties, particularly the hardness, was also expected [6].

W-S-C coatings deposited either by magnetron- assisted pulsed laser deposition or by laser ablation of graphite and WS₂ composite targets were prepared by Zabinski et al [47]. The friction coefficient in dry air was found to be lower than the one measured in humid air (0.02 and 0.15, respectively). This interesting feature, observed during environmental cycling, was dubbed as the "chameleon behaviour". This implied that the low friction in dry air increased in the presence of humid air and fell down when the air was dried again. Cavaleiro et al, have intensively studied W - S - C coatings prepared by magnetron sputtering, including their structure [51], their mechanical properties [52] and their tribological performance [44,53]. Initial set of studies revealed that the W - S - C films were deposited by sputtering from a WS₂ target in a CH₄-containing reactive atmosphere. A large range of chemical compositions from pure WS₂ to W - S - C with carbon contents up to 70 at. % were prepared by varying the flow of the CH₄ and the target power. The S/W ratio was about 1:2 [6]. A nanocomposite WC/DLC/WS₂ coating, deposited by laser ablation from a combined WS₂-graphite target, for aerospace applications was presented by Voevodin et al [48] in 1999. The coating combined the low friction and wear resistance of amorphous diamond-like-carbon with the wear resistance of WC and the solid lubrication of WS₂. These coatings came to be known as "chameleon coatings" due to

their ability of providing low friction in dry conditions and otherwise [47]. Nossa and Cavaleiro, in 2001, gradually added C and N to WS_2 [54]. This was different to the approach of Voievodin et al, where a WS_2 phase was added to DLC and W-doped DLC for lubrication. Increasing the C content changed the microstructure of the coating from columnar WS_x to a dense amorphous carbon matrix with WS_2 nanocrystallites. There was also a definite increase in the mechanical properties of the coatings in that, their hardness reached a maximum for coatings with C between 40-50 at.% [55]. A similar behaviour was observed for the W-S-N coatings.

Further work on W-S-C coatings was carried out by adding Cr and studying its effects on the coating microstructure and behaviour by Polcar et al [56]. Although, the addition of Cr did improve the hardness of the coatings; their tribological behaviour, however, did not get better.

The microstructure of the reactive deposited W-S-C coatings with a high carbon content was reported to be formed by a mixture of nanocrystals of the WS_2 phase along with nanocrystals of the W-C phases and the small C-based amorphous zones or in case of coatings with a low carbon content, just by WS_2 nanograins dispersed in an amorphous carbon matrix [6]. It was reported that coatings such as WS_2 , DLC and WC exhibited a similar behaviour of a huge friction coefficient difference when sliding in humid or dry air [48–50]. The alternative formation of a WS_2 -rich or a C-rich layer during the cyclic change of the environment from dry to humid, respectively, lead to the aforementioned behaviour. Miyake et al [57], presented the concept of nanolayered structured coatings for the TMD+C composite coatings, where the tungsten disulphide and the carbon layers form a "super-lattice" film (with the layers only a few nanometers thick). However, the performance of such films was only average [57]. Figure 2 gives a schematic representation of the W-S-C film designs.

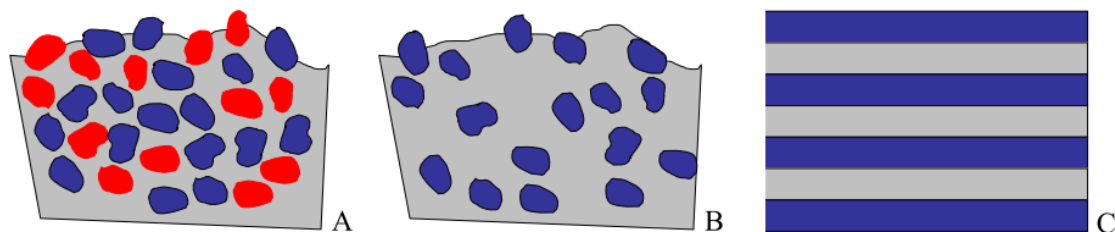


Figure 8 - W-S-C films designs: A) Nanocomposite coatings with hard WC nanoparticles embedded together with WS_2 nanograins in an amorphous carbon matrix); B) nanograins of WS_2 in a C-matrix; C) film with super-lattice $WS_2 + C$ layers [6]

Neither of the coating microstructures shown in Fig. 8 (above) proved to be ideal for reducing the friction coefficient in humid air. In case of a multilayer film, interlayer sliding may occur in the bulk of the film where the shear stresses are larger than at the surface and this makes the multilayer films susceptible to cohesion damage [6]. Thinning of layers down to the nanometer regime, albeit a logical solution, may be difficult to achieve on an industrial substrate. The other two microstructures, on the other hand, could not provide enough evidence in support of the fact that either the TMD nanocrystals could be re-oriented with the basal planes parallel to the sliding distance or the oxidation of the dangling bonds would not occur [6]. Veritably, the extremities of the grains during the

re-orientation process enter directly in contact with the atmosphere resulting in their immediate oxidation [6]. Evidently, for modern low-friction universal coatings exhibiting high wear resistance, load-bearing capacity and, particularly, low friction in various sliding environments (vacuum/dry air or nitrogen/humid air; elevated temperature, etc.), a new concept was required.

The basis to achieve a low friction coating in different environments is a micro/nano structure where the TMD nanocrystals could be deposited completely enrobed in a protective C-rich matrix. Conceivably, if these nanocrystals should have shapes that allow an easy reorientation of the basal planes parallel to the sliding direction then the performance of the coating is enhanced. The carbon matrix contributes towards improving the hardness and the compactness of the coatings but most importantly towards protecting the TMD against oxidation. With this approach, the TMD coating should assure low friction coefficients, not only due to the easy sliding of the basal planes but also due to the existence of only a few strong bonds promoted by the oxygen. Based on this approach, the use of other types of TMDs such as MoSe₂, with less sensibility to the oxidation than tungsten and molybdenum disulphides [16,28] along with the added properties of better mechanical properties and hardness due to the addition of carbon, should also be envisaged.

Strong shear stresses, which are a feature of sliding during pin-on-disk testing, could contribute to the reorientation of the TMD crystals in the C-based amorphous matrix. Nonetheless, their contact with the atmosphere, during the reorientation process, gives rise to the reaction of the dangling bonds of the end planes with oxygen with the subsequent increase of the friction. Pure TMD coatings have a porous structure and therefore, this phenomenon was not observed in them. However, due to their very low hardness they give rise to a very high wear rate. So, with regard to wear models it is expected that the TMD material is worn out which then adheres on both the surfaces in contact. This tribolayer, albeit very thin (nanometer scale), has a highly oriented TMD phase with the basal planes parallel to the film surface [16,58]. Yet another solution to the problem of oxidation is that it could be avoided if the crystals were already aligned in the material, as such a case would present no dangling available for reaction [27]. It was recently proved that during the mechanical deformation of the material by indentation the nanocrystals of a compound, such as TiC, could be rearranged throughout the C-matrix [6]. Consequently, it may be possible that TMD-C films exhibit similar behavior. The re-orientation of TMD crystals in a carbon matrix, however, is a subject that has not been researched yet. TMD-C films, were thus prepared, with very small nanograins of the TMD phase (reduced, if possible, to one cell of TMD). This was so, as easy re-orientation of the TMD phase inside the carbon matrix could be promoted due to its small grain size.

Ambient conditions affect the endurance of tribological applications of layered metal dichalcogenides, of which WS₂ and MoS₂ coatings are used most extensively for tribological applications. According to Ehni *et. al*, better tribological behaviour of such films is observed in dry Ar or vacuum rather than at room atmosphere [59]. A worsening effect of the mechanical and tribological behavior is observed due to the porous morphology of these films, as mentioned earlier in this section, while, the presence of oxygen also undermines their tribological performance, particularly when their friction coefficient is concerned.

Alloying W-S films with other chemical elements or compounds improves their toughness and load bearing capacity [60–62]. Zabinski *et. al*, alloyed the W-S films with the C element [63] which proved, along with previous works of other research groups,

that the C element significantly improves the hardness of the films [48,55]. Also better tribological performance was observed as a direct result of better adhesion of the films with the substrate upon using a Ti interlayer between the same [13]. The structural, morphological and chemical characteristics of W-S films are heavily influenced by the use of different sputtering techniques and deposition parameters [64,65].

2.3 Deposition Methods for W-S-C films

Research on deposition of W-S films for tribological applications has been wide and extensive. Numerous techniques have been employed by various groups in this regard. Some of the earliest works carried out in this field was that of Hirano et al [65] which involved the deposition of WS_2 films by sputtering. Prasad et al [66], reported the feasibility of the pulsed laser deposition (PLD) technique to grow WS_2 films on metal-matrix composite substrates. PLD films were also believed to be more fully dense than sputtered films yet their susceptibility to moisture could not be avoided. The steady-state friction result of this coating against a steel counterface was as low as 0,04. Waghray et al [67] deposited metal chalcogenide solid lubricant thin films using the burnishing as well as the sputtering techniques. DC magnetron sputtering technique, employed by Rai et al [64], to deposit WS_2 is one of the more common deposition techniques used for solid lubricant film deposition. The coatings were then ion-irradiated which resulted in better adhesion and higher hardness. Yet another technique to deposit thin films of WSe_2 was used by Salitra et al [27] which used high temperature selenization of vacuum evaporated WO_3 films on quartz in an open furnace. Interestingly, Voevodin et al [48], prepared nanocomposite coatings made of diamond-like carbon (DLC) and TMD phases for aerospace applications. Such coatings came under the W-S-C material system using a hybrid technique comprising of magnetron sputtering and pulsed laser deposition. Nossa et al [55], deposited Ti/W-S-N and Ti/W-S-C coatings by r.f. magnetron sputtering with different target and substrate holder power supplies. This process, however, showed the presence of oxidation caused due to the contamination of either residual water vapour in the deposition atmosphere or the target. Also preferential resputtering of sulphur by energetic species was employed during deposition to lower the S content with respect to stoichiometry. This clearly shows that the chemical composition of the coatings can be controlled and manipulated according to requirements. Koch et al [68], used the same technique to deposit W-S-C coatings. The only change here was the use of a compound target in the form of WS_2 with CH_4 used as the reactive gas. No substrate bias was applied during deposition. The work of Evaristo et al [52], involved the use of both the reactive and the co-sputtering processes in order to deposit W-S-C films. The reactive process used an Ar + CH_4 atmosphere while, the targets in case of the co-sputtering process were WS_2 and C. An interesting point of difference observed between the two films deposited by the aforementioned processes was that, the films co-sputtered with C were found to be amorphous. However, in case of reactive deposited films, a loss of crystallinity of the film was observed with increasing carbon content thereby clearly showing that both these processes have an effect on the microstructure of the films. MoS_2 coatings, with a mixture of short-range order basal planes and edge-plane oriented grains near the film substrate interface, were deposited using, again, the r.f. magnetron sputtering technique by Doriaswamy et al [69]. Based on this study, they concluded that in order to avoid contamination artefacts that arise due to this process, UHV conditions during deposition was essential. Callisti et al [70] also showed that it was possible to deposit a self-

lubricating W-S-C coating with different Ni-Ti-(Cu) interlayers by magnetron sputtering leading to noticeable microstructural changes which directly influenced mechanical properties of the coatings.

The deposition of coatings on a surface can take place using different methods. Two main categories of the vapour deposition method are chemical vapour deposition (CVD) and physical vapour deposition (PVD). Molecular precursors undergo chemical reactions in order to form the desired coating material in CVD whereas in PVD, the displacement of atoms from the source to the substrate takes place as a result of their removal from the source. Yet another technique used for the deposition of coatings is a process called sputtering where plasma is used to eject source atoms. Sputtering, itself, can be of two types, namely co-sputtering and reactive.

2.3.1 Magnetron Sputtering

The process in which bombardment by energetic particles causes the atoms to eject from a material, is called sputtering. Deposition of coatings can be effectuated by this process. A source material, or a target, releases atoms in the presence of ions of a sputtering gas. The released atoms are then deposited onto a substrate in a vacuum chamber. A vacuum chamber is used to allow the sputtered atoms to reach the substrate surface. The gas used for sputtering is mainly argon (Ar). Formation of a plasma of Ar⁺ ions takes place by discharge and this process is sustained by the ionization of Ar atoms. Magnetron sputtering involves the use of a magnetic field near the target in order to increase the plasma density. As a result of this, an eroded zone is formed on the target and its atoms are sputtered from a so-called racetrack.

Deposition of coatings can take place from elemental or compound targets. Co-sputtering, or the process of sputtering from more than one target, can be employed to vary the coating composition by controlling the current to each target. Not only is the nature of the deposited coating dependent on this, but also on the current, pressure, substrate distance from the target, and so on. The sputtered atoms, on their path towards the substrate, experience collisions leading to a loss of kinetic energy and/or a change of direction. These atoms then get deposited on the substrate by condensing on the surface and losing energy rapidly. The possibility of these atoms to diffuse to energetically favourable positions is low due to the high quench rates. Also, the conditions during sputter deposition are far from a state of thermodynamic equilibrium. Substrate heating can result in the availability of more energy for surface migration leading to a larger degree of crystallisation during the growth of the coating (or film). Application of a negative electrical bias to the substrate in order to induce ion bombardment is also used by many authors for the said purpose. This technique, however, leads to re-sputtering and stresses in the coating.

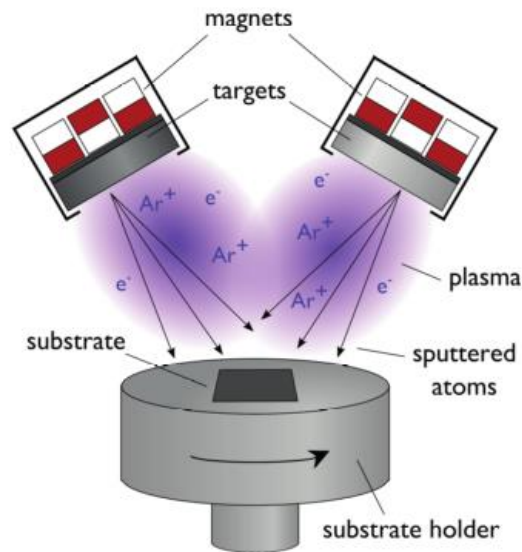


Figure 9 - A magnetron sputtering system during co-sputtering from two targets [2].

The behaviour of the atoms from the target, in their path to the substrate and on the surface of the substrate is affected by the various process parameters. This is different for different atoms and so the composition of a multi-element coating is totally dependent on the process. The composition of a deposited coating, in case of a compound target, often differs from that of the target. The size and mass of the sputtered atoms, during gas phase transport, affects its behaviour in colliding with other atoms and alters its likelihood to reach the substrate. As the so-called sticking coefficient varies between elements, so not all the sputtered atoms reaching the substrate surface actually get deposited. Even after deposition, it is likely that some atoms may be re-sputtered from the surface of the substrate by the incoming atoms from the target. Conventionally, under-represented elements in the coatings are generally the elements that are lighter. For example, coatings that are substoichiometric with respect to S are usually obtained from WS₂ targets.

2.3.2 Reactive Magnetron Sputtering

Desired coating composition is not always possible to obtain from sputtering from one or more targets. Insufficient sputter rates and non-conducting properties of elements (non-metals) so that there is no ignition or maintenance of the plasma are some of the limitations of the co-sputtering method highlighted when used for specific cases. This problem is solved by introducing one element as a reactive gas in a process called reactive magnetron sputtering. While often used to produce carbide (from CH₄ and C₂H₂), nitride (from N₂) or oxide coatings (from O₂); this process involves the ionisation of the reactive gas by the plasma and its subsequent reaction with metal atoms sputtered from a metal target to give rise to a compound coating. The interactions between the gas and the target material take place throughout the chamber. This also leads to the formation of the compound on the target, a process known as poisoning. This can be prevented by supplying a low quantity of the reactive gas to erode the target. Once the target becomes poisoned, there is a drop in the deposition rate as the process goes into the compound mode. Different reactive gas flows causes the transition between metallic and compound mode (depends on increasing or decreasing the flow rate). This is further described as hysteresis.

2.4 Performance of TMD-C Films

The TMD-C (25-70 at. % C) coatings (W-S-C and Mo-Se-C) were tested under different conditions. Polcar et al [71], studied their performance by varying humidity from dry air to 90% relative air humidity as well as temperature from room temperature to 500 °C and concluded that friction in dry air at room temperature is as low as 0,05 while, that at elevated temperatures is even lower. Other parameters that were varied were load (5 N to 48 N) [72], sliding speed (10-1000 mm/s) [73] and test duration (a few thousand to one million) [74]. Findings of note that were reported based on these tests were firstly, friction decreased with increasing load; secondly, coating with carbon content around 50 at.% performed the best under any sliding conditions; thirdly, the friction was found to be humidity-dependent for a short test duration however, TMD-C films have a very long running-in period and the final steady-state friction recorded in humid air was close to that in dry air; finally, 400 °C for W-S-C and 250 °C for Mo-Se-C films were obtained as the functional temperature limits. Under reciprocating sliding conditions (frequency 20 Hz, stroke length – 1mm), coatings with carbon content around 50 at.%, under very high applied loads in humid air, had their friction coefficients approach the values obtained for that in dry air. Therefore, this meant that, re-orienting the TMD nanocrystals in dry air was indeed achievable albeit with a significant amount of energy spent. The TMD phases present in the contact drive the sliding process in this case, which is so typical of TMDs. In pure carbon films, however, the friction values increase with load. So, low friction coefficients for TMD-C coatings, in any environment, could be achieved under sufficient contact pressure or test duration.

Analysis of the top surface of the sliding track after wear testing was done by Polcar [6]. Raman spectra of the TMD-C films (Figure 4) revealed that an increase in load or the number of cycles give rise to a more intense signal of the bands assigned to the TMD phase in comparison to the G and D bands assigned for the C-based material, a result which confirms the increasing agglomeration of TMD materials close to the contact zone. This was suggested by results of Auger spectroscopy chemical depth profiles of the wear track [73,74]. A reduction in friction is only observed, however, when the basal planes of the TMD material in the contact zone are aligned parallel to the surface without the presence of any oxidation leading to any bonding between the same. The resulting tribolayer that is formed is a protective layer, one that is free from the oxidation of the dangling bonds of the original short TMD platelets [6].

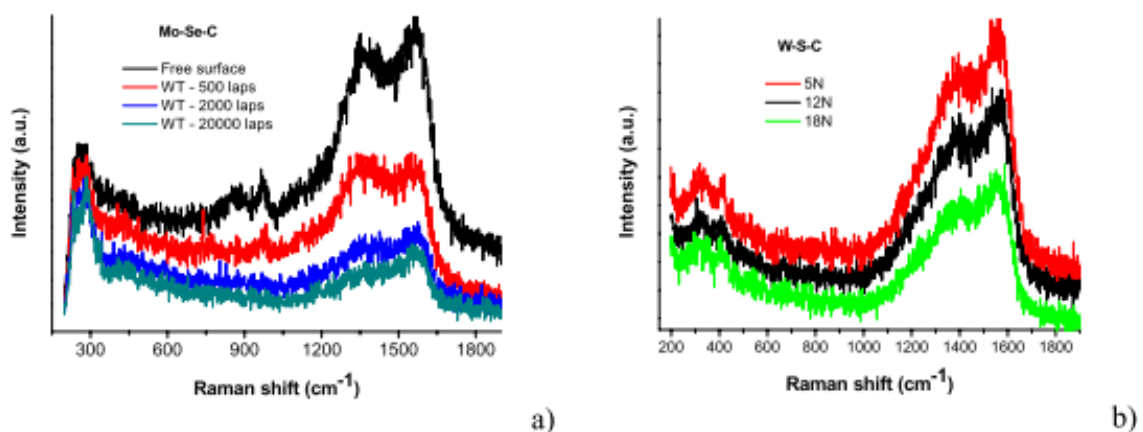


Figure 10 - Raman spectra taken from the center of the wear track as a function of the test duration (a) and applied load (b) [6].

The parallel orientation of the TMD platelets to the surface was revealed by HR-TEM performed by Polcar [6]. The reorientation, in conclusion, was made progressively from some tens of nanometres until the track surface. The orientations encountered in the first 5 nm of the top layer were mostly those that were parallel to the surface and the number of well oriented platelets with basal planes parallel to surface was found to decrease with increasing distance from the surface [6].

2.5 Tribological behaviour of NBR

Moore [75], observed that during sliding, part of the friction coefficient arises from the adhesion between the rubber surface and the substrate. The rest is due to the friction force, which is opposed to the sliding body. For a given rubber, the adhesion component of the coefficient of friction is expressed by the following relation [75]:

$$F_{adh} = K_2 \frac{E'}{p^r} \tan \delta$$

where, p is the normal pressure, r an exponent with a value of 0,2 and K_2 is the constant dependent on the particular sliding combination. Therefore, although a stick-slip process occurs, adhesion is also related to the viscoelastic properties of rubber.

The influence of the ACN content on the tribological behaviour is not properly established and rubber is known to exhibit unusual sliding behaviour due to its very low elastic modulus and the high internal friction in a wide frequency region [76].

Even in the absence of apparent wear, the phenomenon of thermo-oxidation is known to occur at the interface between the rubber and the substrate. This is an oxidation process that occurs due to the friction at the interface between the two solids [10]. The butadiene species in the NBR are sensitive to ageing [77], particularly at high temperatures where this process exhibits drastically [78]. The ACN units remain unaffected by this process [77]. Thermo-oxidation leads to the formation of new groups C=O or C-O on the sample surface, resulting in a higher rigidity and microhardness of the sample surface [10].

Degrange et al [10], observes that the thermal density flow is directly proportional to the value of the coefficient of friction. This implies that rapid thermo-oxidation occurs when a rubber surface receives a great amount of thermal energy [10]. In order to improve rubber surface properties, viscoelastic properties need to be taken into account. A low wear rate is obtained as long as one remains very close to the main relaxation temperature [10].

3. Methodology

3.1 Materials

AISI 316L stainless steel was used as the substrate material for the deposition of the desired coating. This grade of stainless steels are molybdenum-bearing austenitic stainless steels that have better resistance to general corrosion and pitting/crevice corrosion than the conventional chromium-nickel austenitic stainless steels such as Type 304 [79]. The dimensions of the cylindrical steel substrates was diameter, $d = 25$ mm, thickness, $h = 8$ mm. Two different kinds of pins were used as the counter-body for the tests. The diameters of both were 10 mm. The first was an industrial grade acrylonitrile butadiene rubber (NBR) pin whereas, the second was a 100Cr6 steel pin.

Table 2 - Chemical composition of AISI 316L [79].

Designation	Chemical composition % by mass								
AISI No.	C	Si	Mn	P	S	Cr	Mo	Ni	Others
316L	0,03	0,75	2	0,045	0,030	16-18	2-3	10-14	N- 0,1

The three different coatings studied in this work are pure W-S, W-S-C (49 at.% C) and W-S-C (64 at.% C). Three different depositions were performed to deposit these coatings. Each deposition was performed 2 steel discs, two silicon wafers and one steel pellet. The steel discs were used for the pin (ball)-on-disc tests, one silicon wafer each was used for X-ray diffraction and hardness tests respectively and the steel pellet was used for adhesion tests.

3.2 Characterization Methods

3.2.1 Adhesion Test

The adhesion tests were performed on a CSEM REVETEST (S/N – AOO 14-262) equipment. The scratch was made using a Rockwell C indenter with a stylus of 0,2 mm radius. The applied load was gradually increased from 5 to 50 mN at a rate of 5 mN/min. The sliding speed was 10 mm/min.



Figure 11 - The scratch test equipment used for adhesion tests.

3.2.2 X-Ray Diffraction

The XRD measurements in the current work have mainly been carried out on PANalytical X'PERT Pro equipment, with a focusing geometry for θ - 2θ measurements. This instrument uses the Cu $K\alpha$ radiation for X-rays. The scanning angle range was 5 - 75° (2θ).



Figure 12 - The XRD setup used for this work.

3.2.3 Scanning Electron Microscopy

The microstructure characterisation and the analysis of the wear tracks was performed by JEOL JSM 5310 SEM equipment. Oxford X-Max 20 Silicon Drift Detector with a detector size of 20 mm² was used for energy dispersive spectroscopy (EDS) analysis.



Figure 13 - The SEM instrument at IPN, LED & MAT used for studying the structure and the wear tracks of the coatings.

3.2.4 Nanoindentation

The instrument used in this work was equipped with a Berkovich tip. The hardness and Young's modulus are calculated in the instrument software using the Oliver-Pharr method. The presented values are calculated from multiple indentations on each sample.

3.2.5 Ball-on-Disk

The ball-on-disc tests were performed using a home-made test rig. The sliding speed for all the tests was fixed at 0,05 m/s. An initial load of 5 N was changed to 20 N for the latter stages of testing. Similarly, the number of cycles were also changed from 5000 to a maximum of 60000. The frequency was maintained at 40 rpm. Except temperature, other factors such as humidity was not controlled but it remained more or less the same for all tests. An external heating setup was prepared using two commercially sold heating guns that could reach a maximum temperature of 250 °C.



Figure 14 - The home-made pin-on-disk test rig used for studying the tribological behaviour of the coatings against rubber. The setup of the heating apparatus was done in a way to maintain the substrate surface temperature as close to the desired temperature as possible. The maximum temperature used for these tests was 200 °C.

3.2.6 Optical Microscopy

Optical microscopy, useful to study details too small to see with the naked eye, was used to study the details of the wear tracks and the pins after the tribometer tests. The instrument used for this work was manufactured by Leica Microsystems CMS GmbH (Model No.: DM4000 M LED). The resolution used for the images were either 250 or 500 μm .

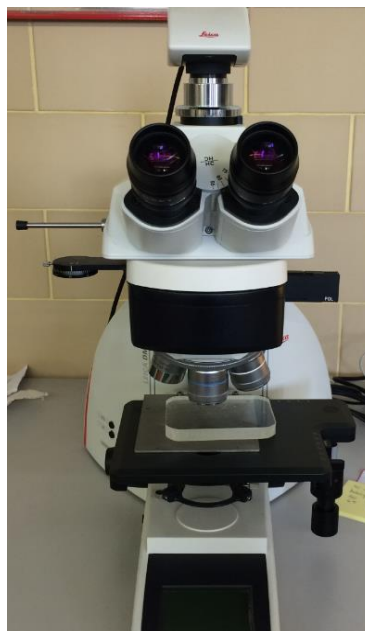


Figure 15 - The optical microscope used in the current work.

4. Results

This work is aimed at studying the tribological behaviour of low-friction transition metal dichalcogenide (TMD) coatings against rubber contacts. More specifically, the goal is to develop an understanding of the mechanical properties and tribological performance of one of such coatings at varied temperatures when used against rubber. The research is primarily focused on triboactive materials. These are materials that actively change in a tribological contact. The study of formation of tribofilms in a tribological contact has also been touched upon. Three different sets of coatings, based on WS_2 , were produced on a 316L steel substrate. These coatings were then tribologically tested, at three different temperatures of 25 °C (RT), 100 °C and 200 °C. The alloyed coatings, W-S-C (49 at.% C) and W-S-C (64 at.% C), from here on will be referred to as WSC49 and WSC64 respectively.

Table 3 - Chemical composition and thickness of W-S-C coatings.

Sample	Power Ratio [P_C/P_{WS_2}]	Chemical Composition				Thickness [μm]
		at.% C	at.% W	at.% S	S/W	
1	0.0	0.0	36.4	59.7	1.6	2.3
2	2.4	48.9	20.4	30.6	1.5	0.9
3	5.5	64.0	21.5	14.4	0.6	1.1

Table 3 presents the total thickness of the coatings as well as their chemical composition, normalized to atomic percent of tungsten (W), sulphur (S) and carbon (C). The film thickness is the lowest for WSC49 while being the highest for the pure WS_2 coating. The S/W ratio decreases with the increase in carbon content for the aforementioned films.

Besides these elements the presence of oxygen was also detected (see Appendix) as is the case with films deposited by co-sputtering. The decrease of O in these films can be associated with the chemical reactions occurring in the chamber during the deposition. The presence of active C species in the discharge atmosphere makes possible the combination with O atoms, forming CO or CO_2 molecules, which are pumped out from the deposition chamber. Also, C alloying improves the coating density thereby, significantly reducing the specific area exposed to the environment. This is another factor in the decrease of O in these films. [52]

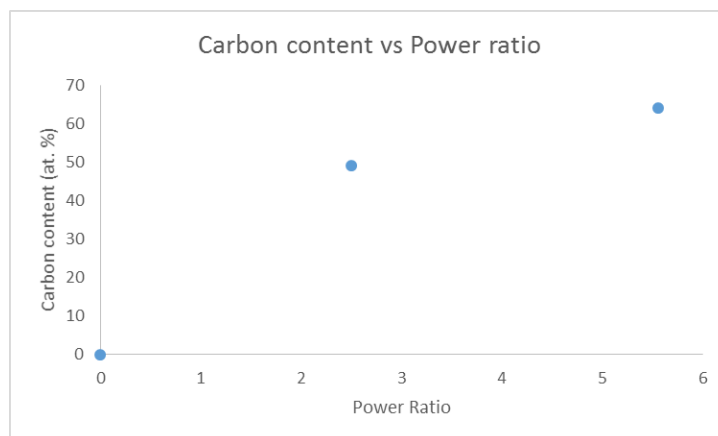


Figure 16 - Carbon content plotted against power ratio.

Figure 16, shows how the carbon content in the films increases on increasing the power ratio. The two W-S-C coatings with different carbon (C) contents were deposited with different C target powers. As expected, increasing the power ratio led to an increase in the C content, up to around 49 at.% C for WSC49 and 64 at.% C for WSC64. For both these coatings, the X-ray diffractograms (Figure 18) showed the expected evolution of structure, starting from a type I WS_x with turbostratic stacking of the (10L) $L=1,2,3\dots$ planes for the pure WS_2 coating.

4.1 Structural Characterisation

The microstructural characterization and film thickness measurements were performed using SEM images. Increasing the carbon content in the film led to an improvement in the compactness of the morphologies of the coating. It has been shown that for contents lower than 30 at.% C, the morphology is columnar (as observed with the pure W-S coating) [52]. In agreement with the work of Cavaleiro et al [51], the increase of the alloying element content (carbon) led to a lower porosity level and to featureless morphologies. The structure of pure WS_2 coatings, as-deposited, was found to be porous, with a columnar morphology, and in some cases very distinct flakes. These coatings have a black and velvet-like appearance, and they can be easily scratched by virtually anything, due to the poor adhesion of the standing flakes [51]. The coating thickness at the center of the sample was observed as 2,3 μm . The thickness decreased considerably to 0,90 and 1,1 μm for WSC49 and WSC64 respectively.

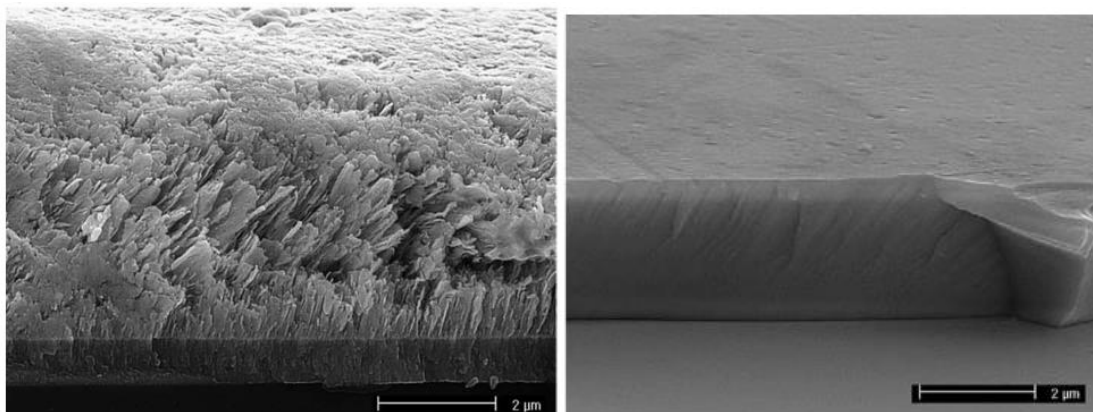


Figure 17 - Cross-sectional SEM micrographs of W-S-C sputtered films deposited with increasing C contents, showing the improvement of the morphology density: pure W-S film (left), W-S-C, 64 at.% C (right).

Figure 18, shows the X-ray diffractogram for the pure WS₂ coating along with spectra for the other samples. The film deposited without C presents the WS₂ phase, with the type I structure (peak (10L) with L=0,1,2, 3 for $2\theta \approx 40^\circ$ and peak (110) for $2\theta \approx 72^\circ$) which is characterized by the (100) planes perpendicular to the substrate surface [80].

The diffraction pattern of the coating, with the two peaks indexed as (100) and (110), is typical for sputtered WS₂. The weak interactions between the sandwich layers in WS₂ cause rotational and/or translational disorder around the c axis, a phenomenon called turbostratic stacking [2,58]. Alloying the films with carbon promotes the loss of crystallinity. The signs of other phases such as W-C compounds can be detected, as observed in similar work done in the past [51]. With the presence of an increasing C content for the alloyed coatings, these peaks become broader with decreasing crystalline domain size. For these films, only one very broad peak is observed at the same positions of the (10L) line of the WS₂ phase. Whatever the C content is, these films present an amorphous structure.

The C-alloyed coatings give broad features at same peak positions, and thus consist of even smaller clusters with limited long-range order. The difference in crystallinity between pure and alloyed coatings can be connected to the increased possibilities for the atoms to diffuse on arrival to the substrate. The W-S coatings from the W-S-C series are all sub-stoichiometric in S, with an S/W ratio of around 1,5 and 0,6 for the coatings alloyed with 49 at.% and 64 at.% of carbon respectively.

The XRD observations were in accordance with the study of SEM cross-sections, showing the microstructure and morphology, of these coatings as reported by Sundberg et al [2]. The X-ray amorphous coatings were reported to be dense and featureless, while the coating with crystalline W-S was flaky and porous. There is a possibility of the W-C phase being present in the coatings, even though no crystalline WC grains are observed by XRD. This has been reported also in other works on W-S-C coatings, where WC nanocrystallites were observed in TEM but not in XRD [47].

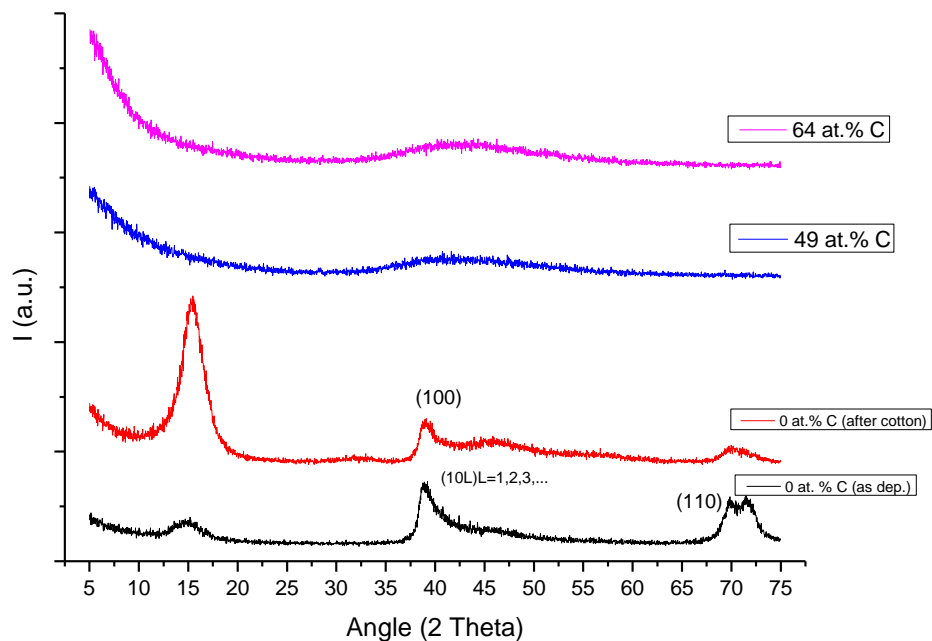


Figure 18 - XRD diffractograms of W-S-C films as a function of carbon content

The amorphous part of the W-S-C coatings should therefore, contain a combination of amorphous carbon and amorphous tungsten carbide.

The evolution of the hardness of the films is presented (Figure 19). The columnar morphology and the high number of pores corresponds to the very low value of the hardness measured in the pure W-S film. This value remained almost the same even after rubbing the sample surface with cotton in one direction. The films with alloyed with C exhibited a marked increase of the hardness in relation to the pure W-S film, in spite of maintaining the columnar morphology. This behaviour is attributed essentially to the modification of the morphology and the structure. The elimination of the typical pores of the columnar morphology gives rise to an increase in compactness and the density of the films, while simultaneously allowing the structure to develop with a strong decrease of the grain size [13].

The highest values of the hardness are reached for the W-S-C films with 64 at.% of C. The coating has a higher amount of amorphous carbon, thus the hardness value tends to get closer to the hardness value of pure C deposited in similar conditions. Previous studies have shown that the formation of W-C compounds allowed to explain the very high hardness of this film [51].

In order to synthesize the C-based phases, mere presence of C content is deemed enough. C-phases in co-deposited W-S-C films have a high number of C-C sp^3 bonds and, consequently, are harder [52].

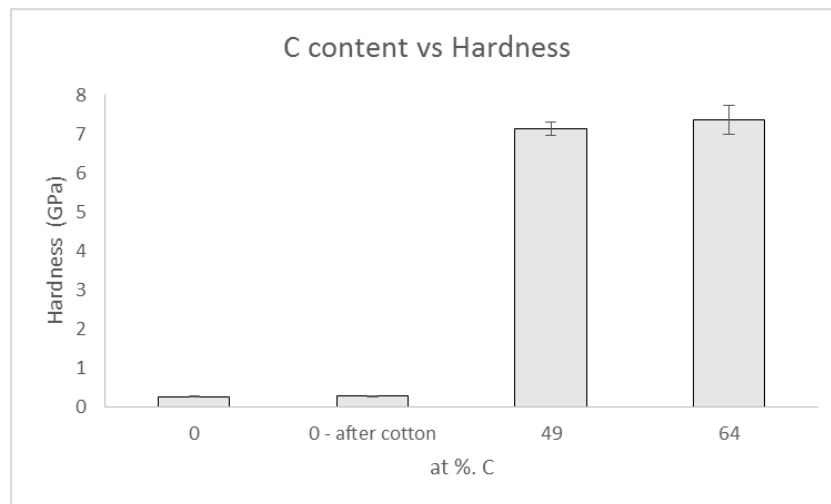


Figure 19 - Mechanical properties of W-S-C films as a function of C content with respect hardness

Table 4 - Mechanical properties of the coatings

	Hardness (GPa)	Critical Load (L _C)
Pure W-S	0,2 ± 0,05	0
WSC49	7,1 ± 0,1	>50
WSC64	7,3 ± 0,3	>50

The hardness values measured in W-S-C films are similar to those obtained by Voevodin et al. [63] in composite films of WC/DLC/WS₂ (60 at.% C) type deposited by pulsed laser deposition, which were close to 7–8 GPa. This hardness, while not comparable to carbides (24–28 GPa), was significantly larger than the typical hardness of solid lubricants, such as WS₂ (around 0,3 GPa), contributing to an increase in their loading bearing capacity. The low hardness value could be justified by the incorporation in the composite of the WS₂ soft phase.

The adhesion of the coatings to the substrate significantly improved upon alloying with C (Table 4). This improvement was attributed to the synergetic effect of the alloyed element, C, and the Ti interlayer leading to the formation of Ti compounds in the interface between the W-S-C films and the Ti interlayer [13]. Interestingly, similar L_C values were reported by Evaristo et al [52], for co-sputtered W-S-C coatings without a Ti interlayer as well.

4.2 Tribological Performance

The mechanism of low-friction, for all WS₂-based coatings in this work, whether binary or ternary, is the formation of the WS₂ tribo-films. The tribological performance of WS₂ coatings is heavily dependent on the nature of the material and the surfaces, as well as on the environment and the contact geometry and load even if their low-friction properties

are well established. The purpose of the current work has been to study the tribological performance of WS₂-based coatings against NBR as the counter body, and understand how it relates to the composition and structure of the coatings, and the conditions, mainly temperature. The friction coefficient measured in ball-on-disc tests is generally dependent on the applied load, i.e. the contact pressure, so that μ is lower for higher normal forces. This work, towards the end, focuses on varying the contact pressure, and for the same reason a much higher load than the one used in the beginning is applied.

The pure W-S and W-S-C coatings were tribologically tested in a pin-on-disc setup with rotating geometry, and at 25 °C (RT), 100 °C and 200 °C. The applied load was 5 N, frequency 40 rpm, sliding speed 0,05 m/s and finally the number of cycles was limited to 5000. At all temperatures, the evaluated pure W-S coating exhibited the lowest and most stable friction with $\mu < 0.4$ when compared with W-S-C coatings. The average friction values, however, expectedly decreased at 100 °C for WSC49 while showing an increase for WSC64. At 200 °C, the general decreasing trend for both these coatings was followed. The friction values for pure WS₂ coating remains more or less the same at all temperatures. The uncoated steel, interestingly, performed better at 100 °C than WSC49 as well as WSC64.

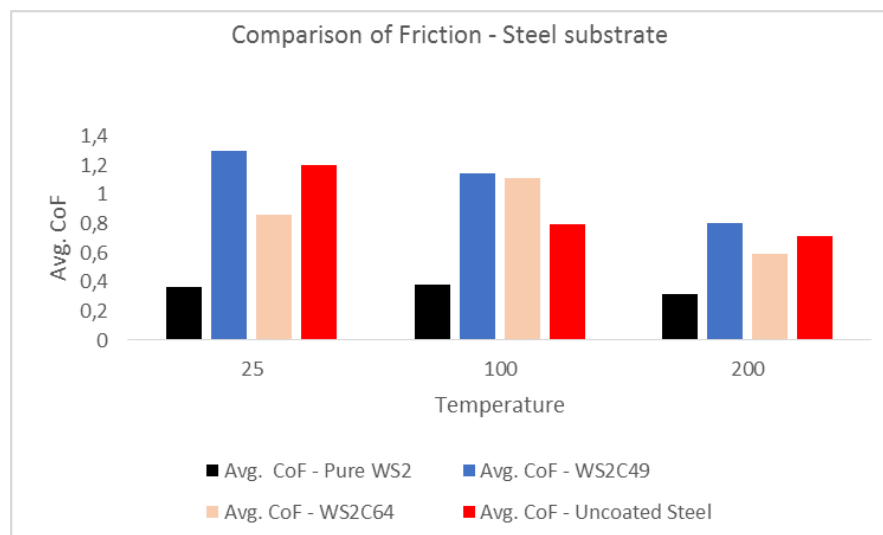


Figure 20 - Comparison of avg. coefficient of friction for the co-deposited coatings at all temperatures.

Figure 20 gives a better idea of the tribological behaviour of the samples at all temperatures. This general trend of decrease in friction with a rise in temperature is attributed to the theory, that the increase of temperature can ease the crystalline slipping of the basal planes that are bonded to each other weakly [81]. Polcar et al. [81], also suggested that the transferable tribo-layer with an hexagonal WS₂ structure is formed in the contact area and that, at increased temperature, intercrystalline slipping of this layer is facilitated.

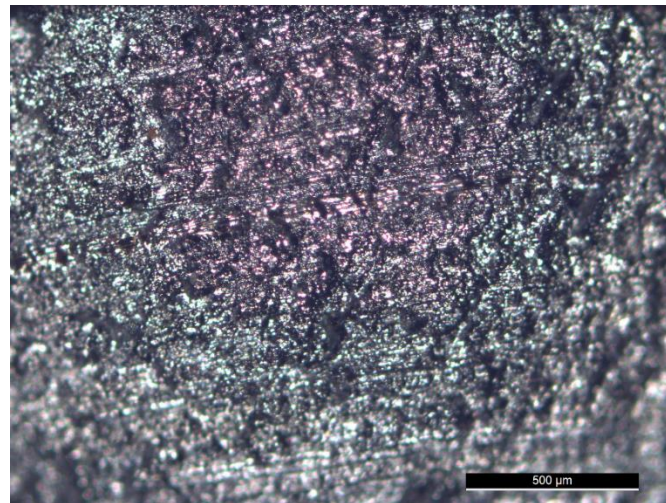
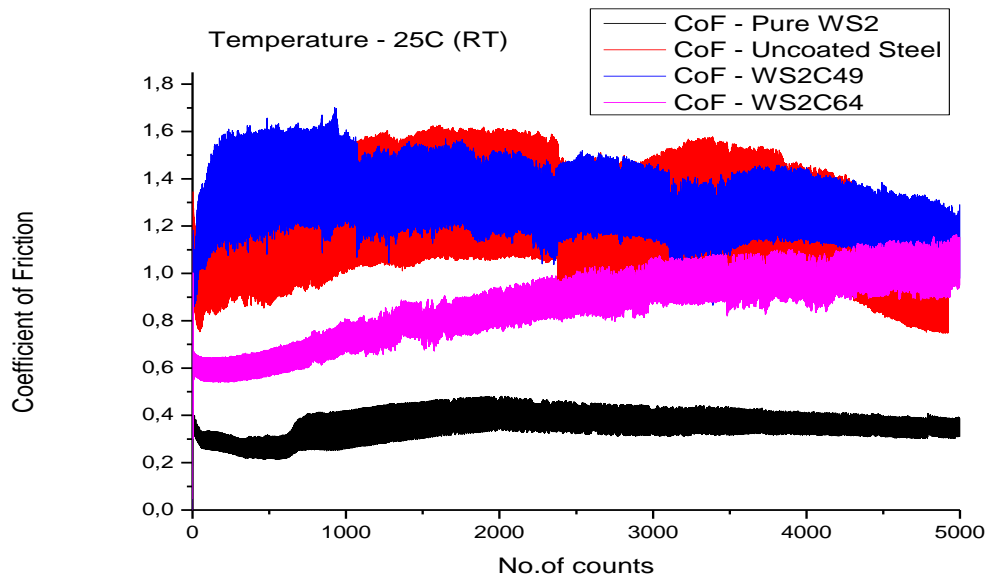


Figure 21 - Friction coefficients of the co-deposited coatings at 25 °C (above). Image of the contact area of the NBR ball taken after the test against pure WS₂ coating showing the presence of a shiny WS₂ tribo-layer on the ball surface (below).

Table 5 - Comparison of friction and wear rates of the co-deposited coatings at 25 °C.

Sample Name	μ	$K [m^3/Nm]$
Pure WS ₂	0,36	$1,5 \times 10^{-13}$
WSC49	1,3	$4,05 \times 10^{-13}$
WSC64	0,8	$4,25 \times 10^{-13}$
Uncoated Steel	1,2	$5,95 \times 10^{-12}$

For the tests run at 25^oC, the pure WS₂ (as-deposited) coating gives the lowest and most stable values of friction ($\mu = 0,36$) (Figure 21, Table 5). As suggested in literature, the presence of a transferable third body, in the form of a WS₂ tribo-film that facilitates sliding, was observed. However, a steady-state was only achieved after around 1000 cycles. The wear rate for this coating on the NBR ball was the lowest compared to the other coatings and the uncoated sample in the study. WSC49 showed a very high friction value and subsequently, the wear on the ball was higher as well. This behaviour was attributed to the absence of the transferable third body as supported by images of the ball taken after the test. Also, no amount of sliding could re-orient the basal planes in the direction of sliding in order to make the sliding process easier. WSC64 started with low values which increased steadily as the test went on. The wear on the ball was slightly higher than the 49 at.% C coating. The highest wear, as expected, was obtained for the uncoated steel.

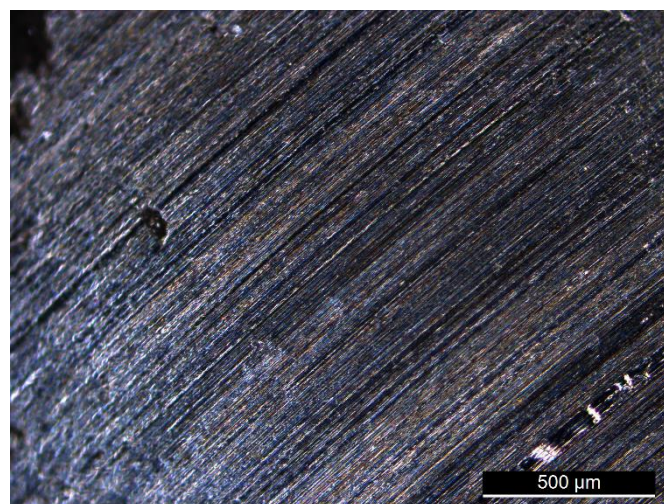
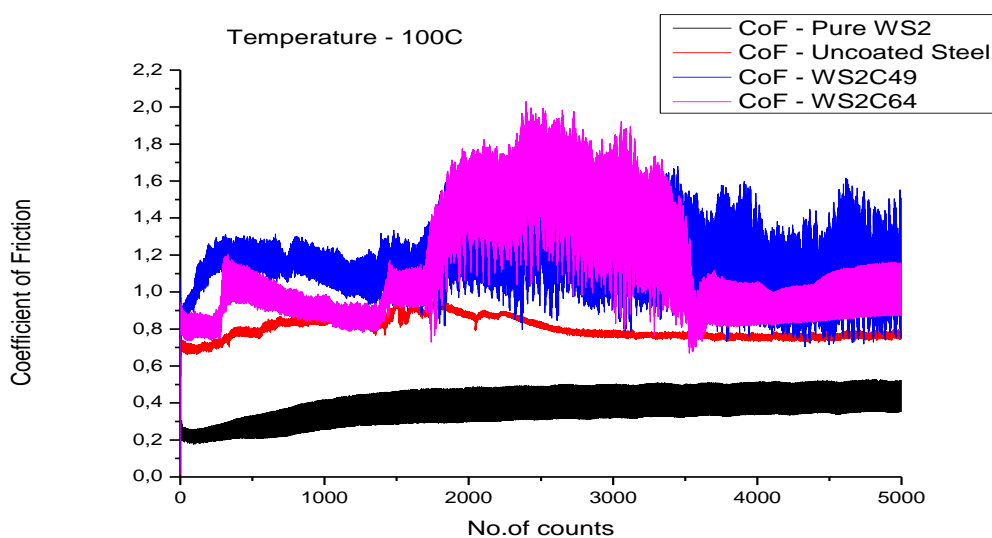


Figure 22 - Friction coefficients of the co-deposited coatings at 100^oC (above). Image of the contact area of the NBR ball taken after the test against pure WS₂ coating showing the presence of a shiny WS₂ tribo-layer on the ball surface (below).

When the tests were run at 100 °C, the pure WS₂ (as deposited) coating again performed the best as compared to the other samples in the study (Figure 22, Table 6). The friction values improved marginally for WSC49 as well as uncoated steel. The appearance of the surface of the ball after the test in both these cases was found to be glossy without any substantial presence of a third body. This suggests that the lowering of friction, no matter how small, was due to the thermo-oxidation of the surface of the ball (at a sustained high temperature) causing it to slide more easily [10]. However, in case of WSC64 the coefficient of friction showed a marked increase against the trend. This behaviour had an effect on the wear rate of the ball used for this sample as well. The wear track on the disc was found to have residue of the ball which was further confirmed by SEM analysis of the said wear track (Figure 23).

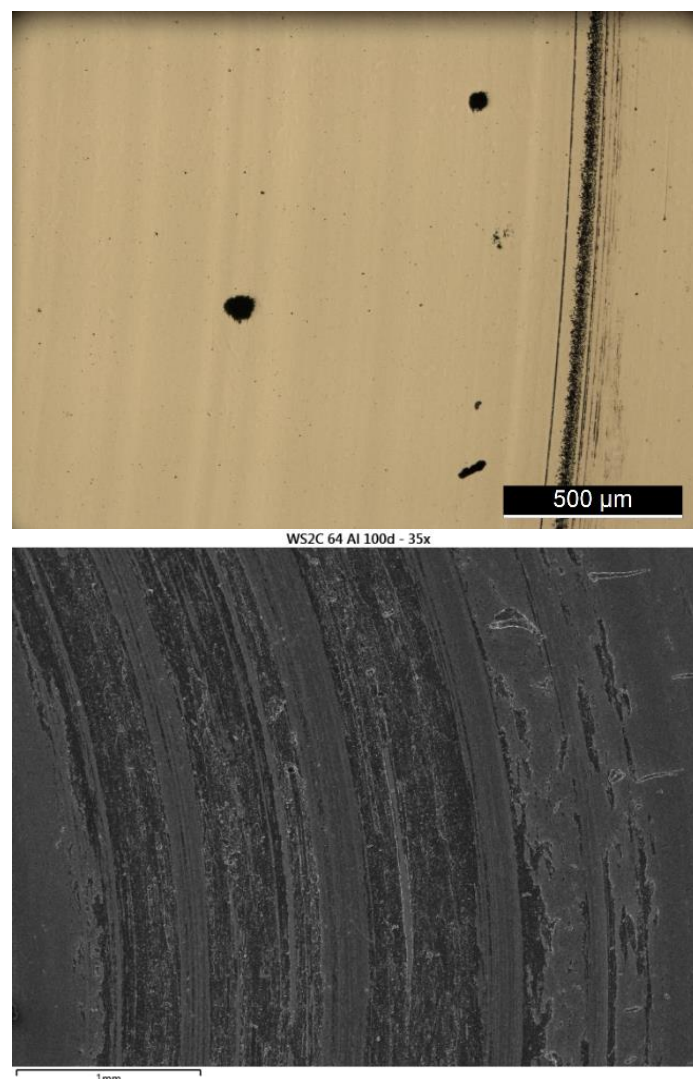


Figure 23 - Wear track for WSC64 against NBR at 100 °C as analysed under a microscope (top) and SEM (bottom).

Table 6 - Comparison of friction and wear rates of the co-deposited coatings at 100 °C.

Sample Name	μ	K [m^3/Nm]
Pure WS ₂	0,38	$1,1 \times 10^{-13}$
WSC49	1,14	$3,5 \times 10^{-13}$
WSC64	1,11	$4,65 \times 10^{-13}$
Uncoated Steel	0,8	$3,42 \times 10^{-12}$

W-S coatings with a high carbon content are known to have high friction and high wear [81]. It may be possible that a high carbon content in the coating enhanced the degradation of the surface of the ball as evident from the rubber residue on the wear track.

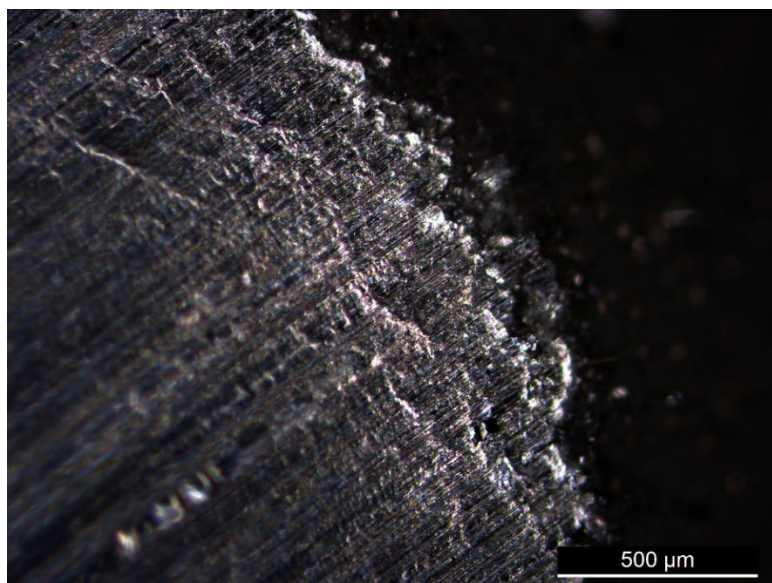
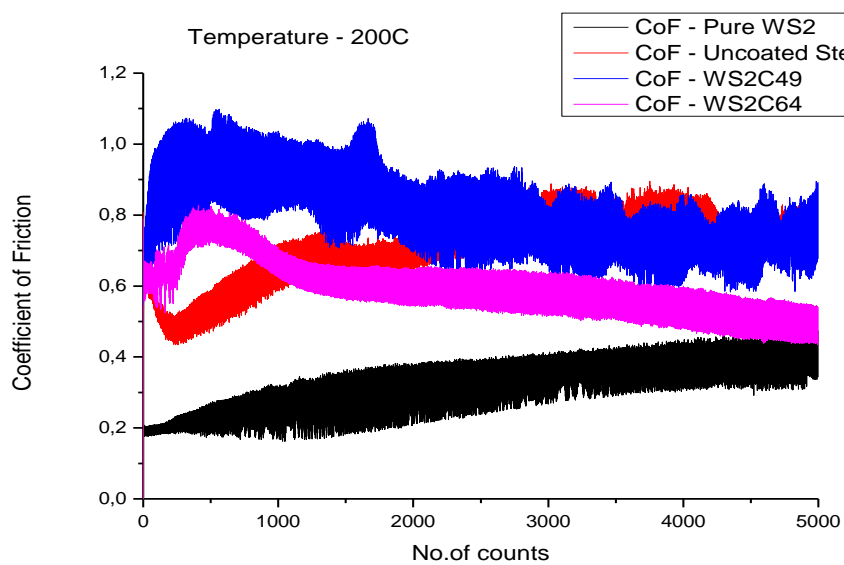


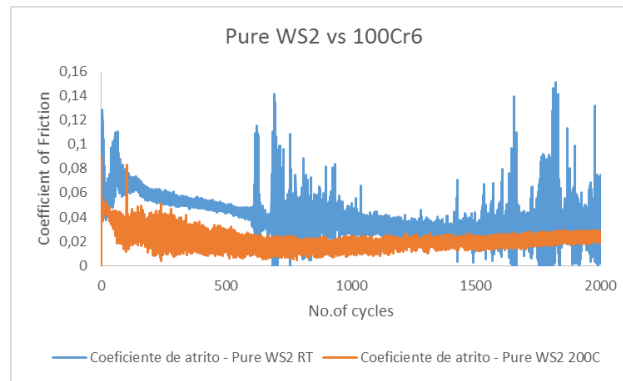
Figure 24 - Friction coefficients of the co-deposited coatings at 200 °C (above). Image of the contact area of the NBR ball taken after the test against pure WS₂ coating showing the presence of a smooth, shiny WS₂ tribo-layer on the ball surface (below).

Table 7 - Comparison of friction and wear rates of the co-deposited coatings at 200 °C.

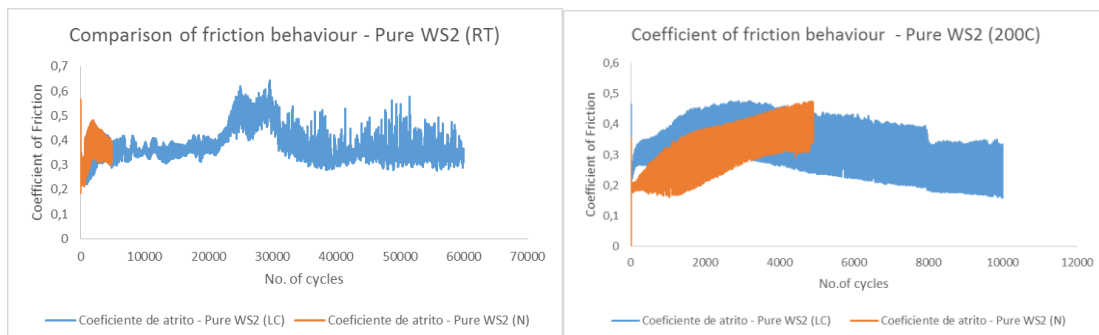
Sample Name	μ	K [m ³ /Nm]
Pure WS ₂	0,32	0,96 x 10 ⁻¹³
WSC49	0,80	0,83 x 10 ⁻¹³
WSC64	0,6	1,25 x 10 ⁻¹³
Uncoated Steel	0,72	1,27 x 10 ⁻¹²

There was a marked decrease in the friction value for the pure WS₂ by almost 0,06 units at 200 °C (Figure 24, Table 7). The appearance of the surface of the ball after the test against this sample was found to be shiny, due to the presence of a third body, as well as smooth. The appearance of the smooth, slippery surface could be due to the high temperature. This suggests that the lowering of friction, in this case, is possible not only due to the presence of the third body but also due to some degradation of the surface of the ball presenting a smooth surface for sliding. The other samples showed similar behaviour of decrease in friction maintaining a coherence with wear rate values for the respective balls used at this temperature. The most significant decrease of friction was observed for WSC64, with the sample recording a decrease of almost 0,5 units as compared to the previous recorded value at 100 °C. The wear track on the discs, in case of both the C-alloyed coatings, was not only found to have a smooth, polished-like finish but also showed no residue of the ball which was further confirmed by SEM analysis of the said wear track.

A further set of pin-on-disc tests were performed. Two notable changes in parameters were made. The applied load was increased to 20 N and the number of cycles to 60000 for 25 °C and 10000 for 200 °C. Another change made in this set of sliding tests was that, a steel (100Cr₆) ball was used for the first 2000 laps in order to promote the re-orientation process of the basal planes in the direction of sliding. This was done as it was believed that occurrence of this process in the previous set of tests was possible and the low friction (achieved only in the case of pure WS₂) was possible only due to the transferable third body. Third body transfer was easier to achieve in this case the flaky, black velvet-like surface of the coating gets worn out easily and acts as a lubricating layer in the contact. However, in case of C-alloyed coatings there was, evidently, no transfer of the third body. Low-friction in such cases can be achieved through re-orientation of the basal planes of the coatings so that they are arranged in the direction of sliding. It was believed that an application of a higher load and higher cycles to facilitate the onset of this process and bring about a marked decrease in friction values.



a)

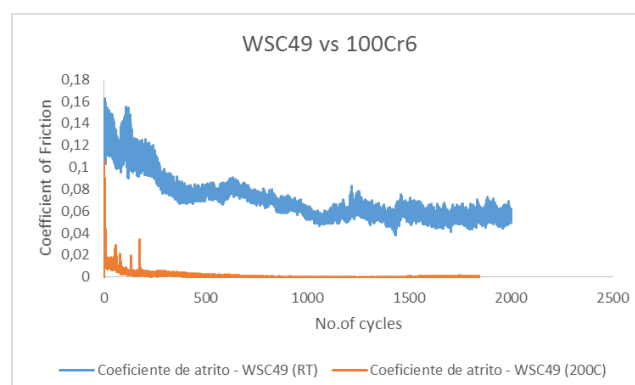


b)

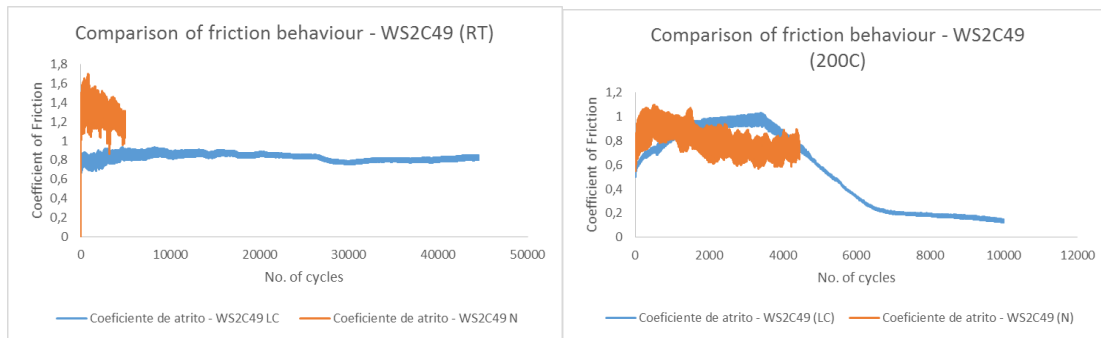
c)

Figure 25 - Comparison of friction: a) friction for 100Cr6 balls at RT and 200C, and friction behaviour of pure WS₂ coating for longer and shorter cycles at b) RT and c) 200C

Pure WS₂ coating when used against a steel ball were found to give coefficients of friction similar to that found in literature [6,81,82]. This suggests that there is nothing wrong with the coating. After the initial sliding with the steel ball, an NBR ball was used and the friction curves from the shorter and the longer cycles were compared at RT and 200 °C (Figure 25 b, c). These curves clearly suggest that the use of the steel ball, for the intended purpose of causing re-orientation of the surface, does not make any difference to the running-in period of the NBR ball.



a)



b)

c)

Figure 26 - Comparison of friction: a) friction for 100Cr6 balls at RT and 200C, and friction behaviour of WSC49 coating for longer and shorter cycles at b) RT and c) 200C

The behaviour of the WSC49 sample when used against a steel ball at room temperature and at elevated temperatures was found to be coherent to literature just like the pure W-S coating [6,81,82], further suggesting that there was no fundamental problem with the deposition procedure or later on with the coating. The friction values for WSC49 against a steel ball at 200 °C reached a steady-state after 150 revolutions. The coefficient of friction was very stable after that. The average value of the coefficient of friction recorded for this test was 0,001 which is even better than some findings. After the initial sliding with the steel ball, an NBR ball was used and the friction curves from the shorter and the longer cycles were compared at RT and 200 °C (Figure 26 b, c). In case of Fig. 26.b), it is possible that the use of the steel ball does have an effect on the running-in process for the NBR ball is used later on. From the aforementioned graph it is clear that the friction is stable and constant from the start of the test. Figure 26. c), shows a steady decline in the friction when the NBR ball was used right after the test with the steel ball at 200 °C. This test started at a friction value lower than the normal test conducted previously with shorter cycles. This should clearly suggest some re-orientation of the surface as a similar case was observed for the test conducted at room temperature (Fig. 26.b). Most significantly and interestingly, however, was the steady decline in the friction value so that the test ended with a recorded friction value of 0,13. Upon investigation, the ball showed signs of degradation and the presence of a very smooth surface, which could have aided the steady decline in the friction. Also, was present, a layer of the third body on the surface of the ball as can be seen from the images (Fig. 27).

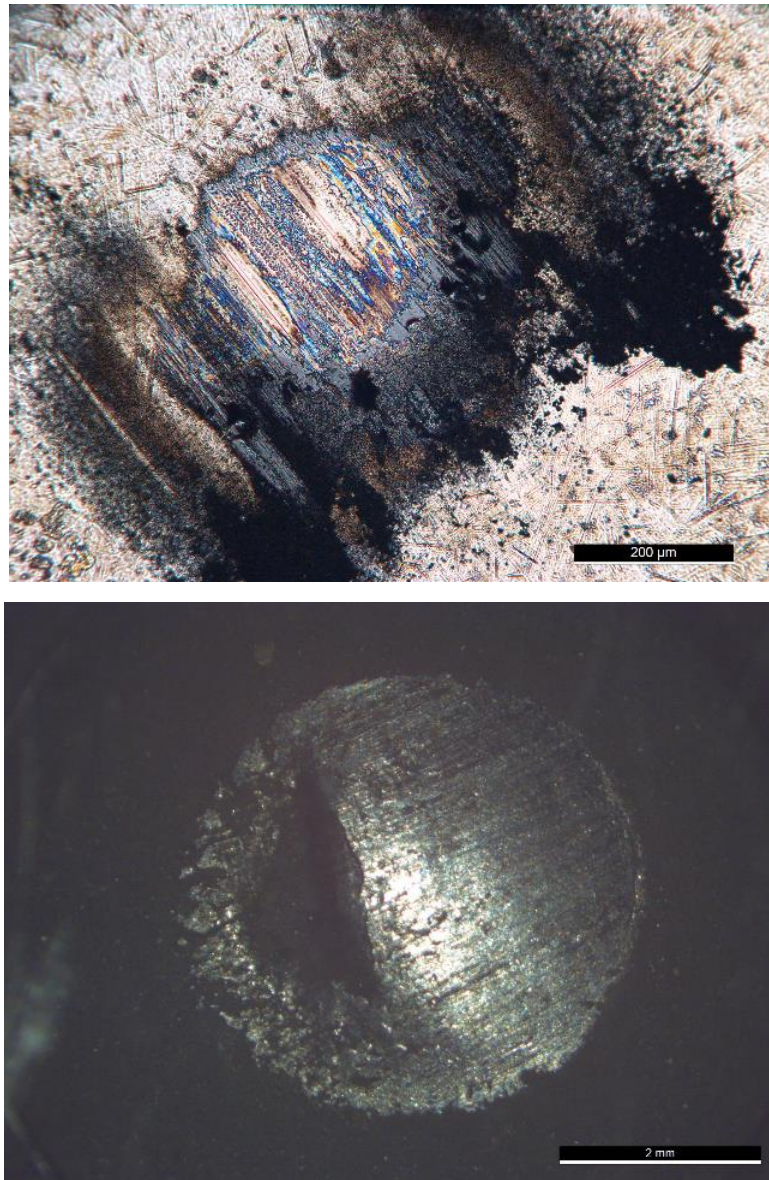
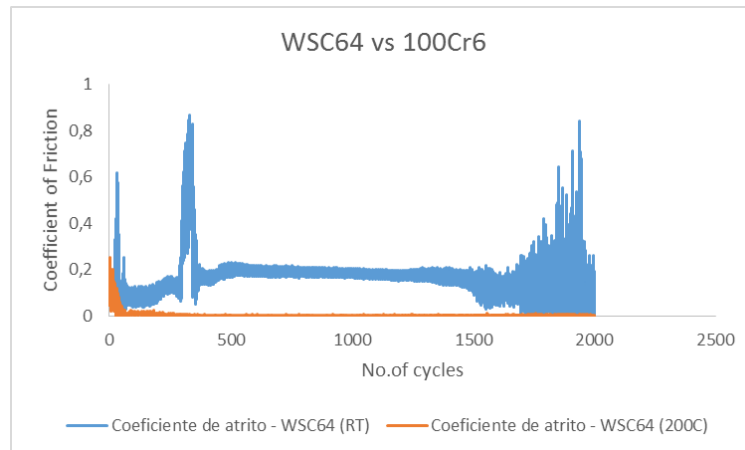
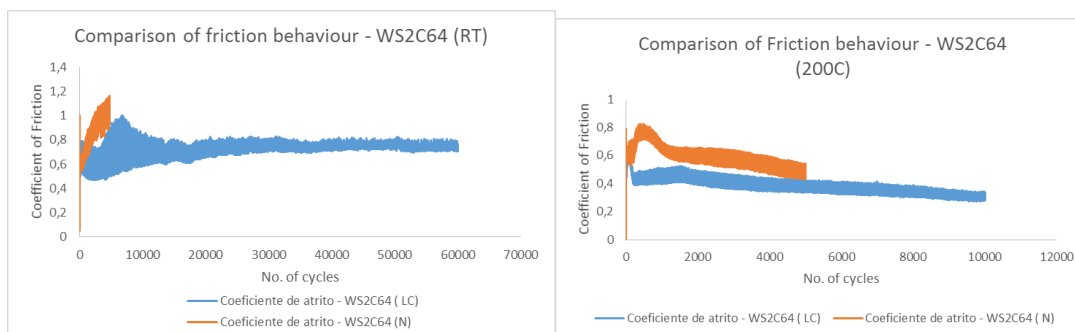


Figure 27 - Images of the 100Cr6 (top) and NBR (bottom) balls taken after test on WSC49 at 200 °C with longer cycles.

The last set of tests were conducted for the sample with the highest carbon content. WSC64 sample when used against a steel ball at room temperature and at elevated temperatures was found to be coherent to literature just like its pure and low carbon counterparts. This again provided strong evidence regarding the appropriateness of the coatings. The friction values for WSC64 against a steel ball at 200 °C took around 400 revolutions to reach the steady-state. However, once reached the friction values were very stable and the average coefficient of friction after 2000 laps was recorded at 0,004. After the initial sliding with the steel ball, an NBR ball was used and the friction curves from the shorter and the longer cycles were compared at RT and 200 °C (Figure 28.b, c). In case of Fig. 28.b), it is possible that the use of the steel ball does have an effect on the running-in process for the NBR ball used later on. Once the steady-state is achieved, the friction values become more stable and constant.



a)



b)

c)

Figure 28 - Comparison of friction: a) friction for 100Cr6 balls at RT and 200C, and friction behaviour of WSC64 coating for longer and shorter cycles at b) RT and c) 200 °C

Figure 28. c), shows a steady decline in the friction when the NBR ball was used right after the test with the steel ball at 200 °C. This test started at a friction value lower than the normal test conducted previously with shorter cycles. This should clearly suggest some re-orientation of the surface as a similar case was observed for the test conducted at room temperature (Fig. 28.b). This time, however, there was the slow decline in the friction value so that the test ended with a recorded friction value of close to 0.2. Upon investigation, the ball showed signs of degradation and the presence of a very smooth surface, which could have aided the decline in the friction. Also, was present, a layer of the third body on the surface of the ball as can be seen from the optical images (Fig. 29). As is evident from Fig. 27 & 29, the wear on the steel ball is much higher when used against WSC64 than when used against WSC49.

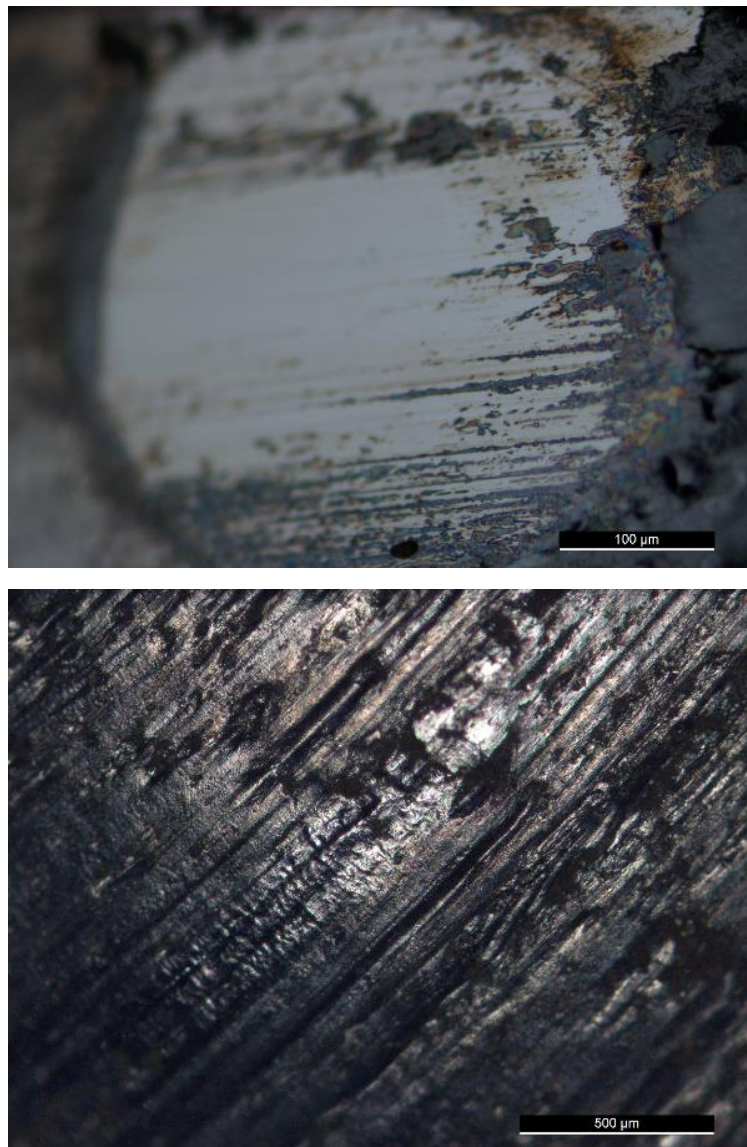


Figure 29 - Images of the 100Cr6 (top) and NBR (bottom) balls taken after test on WSC64 at 200 °C with longer cycles.

The presence of a third body in the form of a transferable tribo-layer, which was very apparent at all temperatures for the test involving the pure WS₂, became less apparent for the WSC49 coating while only appearing for its test with longer cycles at maximum temperature. For the WSC64 coatings, it is safe to say that due to the high carbon content there is no transfer of the third body to the surface of the ball. These facts were confirmed from the optical images as well as SEM.

EDX analysis of the wear tracks for WSC64 coatings showed NBR residue in the form of Ca along with the presence of C, O (see Appendix). The appearance of Ca is due to the rubber pin used. Ca is an important element used in the processing of NBR rubber. The presence of Ca in the wear track suggests wear of the NBR rubber pin. Amorphous carbon was detected, more so for the C-rich coatings where it was present already in the as-deposited state. The presence of O is understandable as it occurs due to the oxidation of the coating. The wear trend of the ball was in agreement with the friction behaviour of

the coatings. The wear on the tracks were too minimal to be studied. Figure 30, summarises the change of friction with temperature.

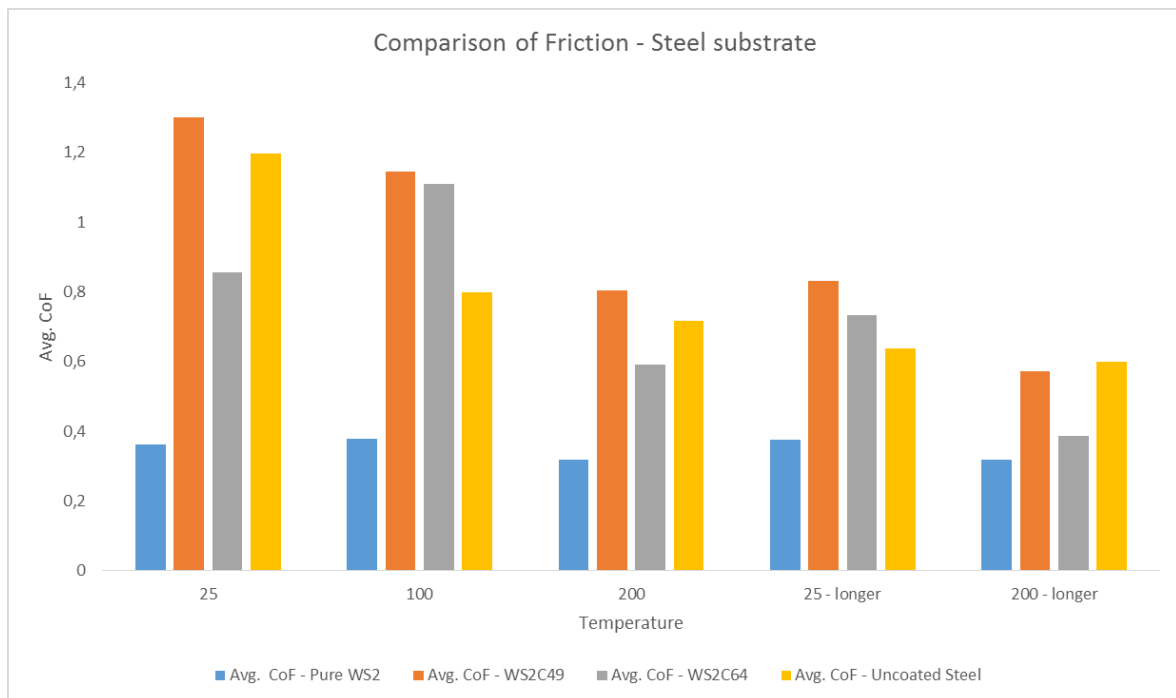


Figure 30 - Friction comparison chart for tests at all temperatures.

W, S and O were detected by SEM analysis in the wear scars on the coatings used for tests performed at temperature. Coatings with a high content of C did, however, not exhibit low friction, which is not surprising given that their W and S content is low. Humidity was one factor which was not controlled for all the tests. Pure W-S coatings were the only ones that performed in agreement with literature on the behaviour of the said coatings. For the other coatings, containing C in various amounts, the composition and conditions apparently did not allow for the formation of a stable WS₂ tribofilm. The low friction of the coatings was attributed to WS₂ tribofilm formation. This is also in agreement with the results of Polcar et al [83]. The analysis of the specific wear rates of the counter-body revealed a correspondence with the friction levels. This implied that low friction was associated with low wear, and high friction with high wear.

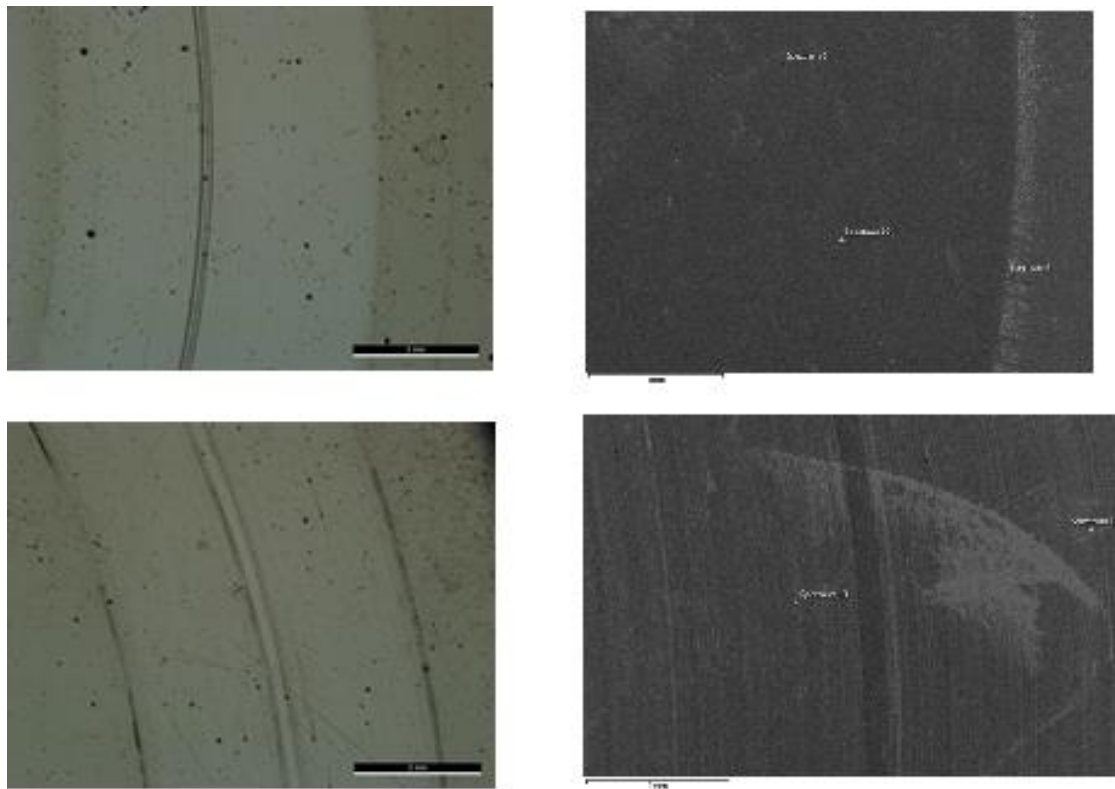


Figure 31 - Optical and SEM images of the wear tracks of WSC49 coating at 200 °C (top) and WSC64 coating at 200 °C (bottom) for longer cycles.

An exception to this was the pure W-S coating, as it exhibited low friction and low wear of the counter-surface, but high wear of the coating itself. Pure W-S coatings exhibit this behaviour which can be explained due to their porosity, poor adhesion, and low hardness. The sliding takes place in a WS₂ tribofilm even when the coating is severely worn as WS₂ still remains in the contact.

For the WSC49 coatings, WS₂ was detected in the tribofilm on the ball only at 200 °C and for a longer run of the test (Figure 31). In the steady-state low-friction regime, after 5000 revolutions, the tribofilm contained crystalline WS₂ platelets, horizontally aligned on the surface. The rest of the tribofilm was found to be made up of a mixture of amorphous and crystalline metal oxide, possibly WO₃.

5. Conclusion

In conclusion, the presence of nanocrystalline WS_x in a matrix of amorphous C and amorphous carbide was achieved by the addition of C to WS_x coatings. A higher C content not only results in the low surface mobility but also the interference of C atoms hinders the formation of WS_x crystallites during deposition. The addition of C was intended to change the mechanical properties, and such an effect is indeed observed. The W-S-C coatings are harder and show better adhesion than pure W-S, with the hardness values in the range of 7-7,4 GPa which can be ascribed to a denser microstructure.

WS_2 , found on the outermost surface in the steady-state friction regime, is continuously removed and re-formed. Another reason for the exceptionally high initial friction levels could be the presence of oxides on the outermost surface of the as-deposited coating, which must be removed before W and S are accessed for formation of WS_2 . Higher friction during running-in, and less stable friction in the steady-state regime is a direct result of the presence of a metal prone to oxide formation, like Ti or Cr [2]. However, low friction values and WS_2 lubrication can still be achieved.

The intended mechanism of low friction for pure and alloyed WS_2 -based coatings, is the formation of WS_2 tribofilms on the outermost surface. The basal planes of these tribofilms are horizontally aligned which results in their easy shearing and ease of sliding along that direction. To have crystalline and horizontally aligned WS_2 in the as-deposited coating is not necessary. For Type-I crystalline coatings (pure W-S coating), i.e. with standing platelets, the basal planes realign in the direction of sliding, while for secondary coatings (amorphous or poorly crystalline) there is a rearrangement of the planes in the contact. Nanocrystalline WS_x grains may or may not be present in ternary or quaternary WS_2 -based coatings. However, WS_2 tribofilms formation is true in both cases by reorientation of the basal planes during the running-in period in order to realign them in the direction of sliding.

Studies have shown that only a few layers of WS_2 are actually needed to provide low-friction [2]. A large number of wear tracks were studied using SEM-EDS, and while it was clear that the presence of a WS_2 tribofilm is connected to low friction, a stronger WS_2 signal is not necessarily related to a better performance. It was also observed that low friction by WS_2 lubrication was observed in contacts that were entirely accommodated in the WS_2 tribofilm [2]. In conditions that have O_2 , sliding takes place in WO_3 , formed as a result of oxidation of WS_2 . The shear strength of WS_2 is increased in the presence of H_2O (in conditions with high humidity), leading to higher friction levels [2]. The presence of O_2 and/or H_2O increases the wear of the tribofilm, and thus also the demands on the supply of W and S from the coating for re-formation of WS_2 [2]. WS_2 may also be formed from W and S originating from different sources. However, it is believed that WS_2 could not be observed when W was present as a compound and in lower concentration, in WC and 316-L steel, respectively [2]. The formation of sulfide from such compounds was thus not energetically favorable enough [2]. The ease of formation and alignment of WS_2 tribofilms, even with a rubber ball, and the resulting low and stable friction, is striking, especially in pure W-S coatings. However, while WS_2 third body layer is often easily formed, their functionality when the coating is alloyed, with carbon in this case, and their subsequent use against NBR remain a question to solve.

6. References

- [1] Holmberg, K., Andersson, P., and Erdemir, A., 2012, “Global energy consumption due to friction in passenger cars,” *Tribol. Int.*, **47**(MARCH), pp. 221–234.
- [2] Sundberg, J., 2014, “Triboactive Low-Friction Coatings Based on Sulfides and Carbides.”
- [3] Madhukar, A., 1975, “Structural classification of layered dichalcogenides of group IV B, V B and VI B transition metals,” *Solid State Commun.*, **16**(4), pp. 383–388.
- [4] Lancaster, J. K., 1990, “A review of the influence of environmental humidity and water on friction, lubrication and wear,” *Tribol. Int.*, **23**, pp. 371–389.
- [5] Martin, J. M., Donnet, C., Le Mogne, T., and Epicier, T., 1993, “Superlubricity of molybdenum disulphide,” *Phys. Rev. B*, **48**(14), pp. 10583–10586.
- [6] Polcar, T., 2009, “Self-lubricating nanostructured coatings based on transition metal dichalcogenides alloyed with carbon,” Czech Technical University.
- [7] Birkholz, M., 2006, *Thin Film Analysis by X-Ray Scattering*, Weinheim.
- [8] Williamson, G. ., and Hall, W. ., 1953, “X-ray line broadening from filed aluminium and wolfram,” *Acta Metall.*, **1**(1), pp. 22–31.
- [9] Oliver, W. C., and Pharr, G. M., 1992, “An improved technique for determining hardness and elastic modulus using load and displacement sensing indentation experiments,” *J. Mater. Res.*, **7**(06), pp. 1564–1583.
- [10] Degrange, J. M., Thomine, M., Kapsa, P., Pelletier, J. M., Chazeau, L., Vigier, G., Dudragne, G., and Guerbé, L., 2005, “Influence of viscoelasticity on the tribological behaviour of carbon black filled nitrile rubber (NBR) for lip seal application,” *Wear*, **259**(1-6), pp. 684–692.
- [11] Harben, P. W., and Dickson, E. M., “Rubber,” pp. 1327–1335.
- [12] Sales, S., 2005, “Acrylonitrile-Butadiene Rubber (Nbr)” [Online]. Available: https://www.surplussales.com/Rubber-Plastic/pdf/rps-footrub-33_properties.pdf. [Accessed: 08-Jul-2015].
- [13] Nossa, A., Cavaleiro, A., Carvalho, N. J. M., Kooi, B. J., and De Hosson, J. T. M., 2005, “On the microstructure of tungsten disulfide films alloyed with carbon and nitrogen,” *Thin Solid Films*, **484**(1-2), pp. 389–395.
- [14] Bhushan, B., and Gupta, B. K., 1991, *Handbook of Tribology - Materials, Coatings and Surface Treatments*, McGraw-Hill Inc., USA.

- [15] M.F. Cardinal, P.A. Castro, J. Baxi, H. Liang, F. J. W., 2009, "No Title," *Surf. Coatings Technol.*, **204**, p. 85.
- [16] A.R. Lansdown, 1999, "Molybdenum Disulphide Lubrication," (Elsevier).
- [17] Rapoport, L., Bilik, Y., Feldman, Y., Homyonfer, M., Cohen, S. R., and Tenne, R., 1997, "Hollow nanoparticles of WS₂ as potential solid-state lubricants," *Nature*, **387**(6635), pp. 791–793.
- [18] Chhowalla, M., and Amaratunga, G. A. J., 2000, "Thin films of fullerene-like MoS₂ nanoparticles with ultra-low friction and wear," *Nature*, **407**(6801), pp. 164–167.
- [19] Remškar, M., 2004, "Inorganic Nanotubes," *Adv. Mater.*, **16**(17), pp. 1497–1504.
- [20] Akbulut, M., Belman, N., Golan, Y., and Israelachvili, J., 2006, "Frictional Properties of Confined Nanorods," *Adv. Mater.*, **18**(19), pp. 2589–2592.
- [21] Regula, M., Ballif, C., Moser, J. H., and Lévy, F., 1996, "Structural, chemical, and electrical characterisation of reactively sputtered WS_x thin films," *Thin Solid Films*, **280**(1-2), pp. 67–75.
- [22] Buck, V., 1987, "Preparation and properties of different types of sputtered MoS₂ films," *Wear*, **114**(3), pp. 263–274.
- [23] Muratore, C., and Voevodin, A. A., 2009, "Control of molybdenum disulfide basal plane orientation during coating growth in pulsed magnetron sputtering discharges," *Thin Solid Films*, **517**(19), pp. 5605–5610.
- [24] Lauwerens, W., Wang, J., Navratil, J., Wieërs, E., D'haen, J., Stals, L. ., Celis, J. ., and Bruynseraede, Y., 2000, "Humidity resistant MoS_x films prepared by pulsed magnetron sputtering," *Surf. Coatings Technol.*, **131**(1-3), pp. 216–221.
- [25] Hirvonen, J.-P., Koskinen, J., Jervis, J. R., and Nastasi, M., 1996, "Present progress in the development of low friction coatings," *Surf. Coatings Technol.*, **80**(1-2), pp. 139–150.
- [26] Scharf, T. W., Rajendran, A., Banerjee, R., and Sequeda, F., 2009, "Growth, structure and friction behavior of titanium doped tungsten disulphide (Ti-WS₂) nanocomposite thin films," *Thin Solid Films*, **517**(19), pp. 5666–5675.
- [27] Salitra, G., Hodes, G., Klein, E., and Tenne, R., 1994, "Highly oriented WSe₂ thin films prepared by selenization of evaporated WO₃," *Thin Solid Films*, **245**(1-2), pp. 180–185.
- [28] Kubart, T., Polcar, T., Kopecký, L., Novák, R., and Nováková, D., 2005, "Temperature dependence of tribological properties of MoS₂ and MoSe₂ coatings," *Surf. Coatings Technol.*, **193**(1-3), pp. 230–233.

- [29] Lévy, F., and Moser, J., 1994, "High-resolution cross-sectional studies and properties of molybdenite coatings," *Surf. Coatings Technol.*, **68-69**, pp. 433–438.
- [30] Teer, D. G., 2001, "New solid lubricant coatings," *Wear*, **251**(1-12), pp. 1068–1074.
- [31] Savan, A., Simmonds, M. C., Huang, Y., Constable, C. P., Creasey, S., Gerbig, Y., Haefke, H., and Lewis, D. B., 2005, "Effects of temperature on the chemistry and tribology of co-sputtered MoS_x-Ti composite thin films," *Thin Solid Films*, **489**(1-2), pp. 137–144.
- [32] Renevier, N. ., Fox, V. ., Teer, D. ., and Hampshire, J., 2000, "Coating characteristics and tribological properties of sputter-deposited MoS₂/metal composite coatings deposited by closed field unbalanced magnetron sputter ion plating," *Surf. Coatings Technol.*, **127**(1), pp. 24–37.
- [33] Renevier, N. ., Hampshire, J., Fox, V. ., Witts, J., Allen, T., and Teer, D. ., 2001, "Advantages of using self-lubricating, hard, wear-resistant MoS₂-based coatings," *Surf. Coatings Technol.*, **142-144**, pp. 67–77.
- [34] Holbery, J. D., Pflueger, E., Savan, A., Gerbig, Y., Luo, Q., Lewis, D. B., and Munz, W.-D., 2003, "Alloying MoS₂ with Al and Au: structure and tribological performance," *Surf. Coatings Technol.*, **169-170**, pp. 716–720.
- [35] Mikhailov, S., Savan, A., Pflüger, E., Knoblauch, L., Hauert, R., Simmonds, M., and Van Swygenhoven, H., 1998, "Morphology and tribological properties of metal (oxide)–MoS₂ nanostructured multilayer coatings," *Surf. Coatings Technol.*, **105**(1-2), pp. 175–183.
- [36] Wahl, K. J., Seitzman, L. E., Bolster, R. N., and Singer, I. L., 1995, "Low-friction, high-endurance, ion-beam-deposited Pb□Mo□S coatings," *Surf. Coatings Technol.*, **73**(3), pp. 152–159.
- [37] Wahl, K. ., Dunn, D. ., and Singer, I. ., 1999, "Wear behavior of Pb–Mo–S solid lubricating coatings," *Wear*, **230**(2), pp. 175–183.
- [38] Su, Y. ., and Kao, W. ., 2003, "Tribological behaviour and wear mechanism of MoS₂–Cr coatings sliding against various counterbody," *Tribol. Int.*, **36**(1), pp. 11–23.
- [39] Simmonds, M. ., Savan, A., Pflüger, E., and Van Swygenhoven, H., 2000, "Mechanical and tribological performance of MoS₂ co-sputtered composites," *Surf. Coatings Technol.*, **126**(1), pp. 15–24.
- [40] Prasad, S. ., McDevitt, N. ., and Zabinski, J. ., 2000, "Tribology of tungsten disulfide–nanocrystalline zinc oxide adaptive lubricant films from ambient to 500°C," *Wear*, **237**(2), pp. 186–196.

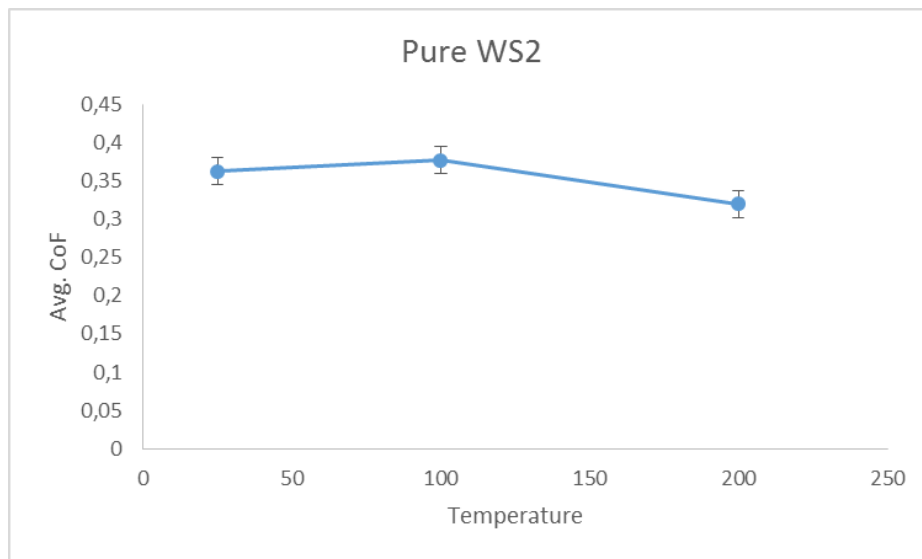
- [41] Zabinski, J. S., Donley, M. S., and McDevitt, N. T., 1993, "Mechanistic study of the synergism between Sb₂O₃ and MoS₂ lubricant systems using Raman spectroscopy," *Wear*, **165**(1), pp. 103–108.
- [42] Prasad, S. ., McDevitt, N. ., and Zabinski, J. ., 1999, "Tribology of tungsten disulfide films in humid environments:," *Wear*, **230**(1), pp. 24–34.
- [43] Zabinski, J. S., Donley, M. S., Dyhouse, V. J., and McDevitt, N. T., 1992, "Chemical and tribological characterization of PbO-MoS₂ films grown by pulsed laser deposition," *Thin Solid Films*, **214**(2), pp. 156–163.
- [44] Nossa, A., and Cavaleiro, A., 2003, "Mechanical behaviour of W–S–N and W–S–C sputtered coatings deposited with a Ti interlayer," *Surf. Coatings Technol.*, **163-164**, pp. 552–560.
- [45] Efeoglu, I., Baran, Ö., Yetim, F., and Altıntaş, S., 2008, "Tribological characteristics of MoS₂–Nb solid lubricant film in different tribo-test conditions," *Surf. Coatings Technol.*, **203**(5-7), pp. 766–770.
- [46] Arslan, E., Baran, Ö., Efeoglu, I., and Totik, Y., 2008, "Evaluation of adhesion and fatigue of MoS₂–Nb solid-lubricant films deposited by pulsed-dc magnetron sputtering," *Surf. Coatings Technol.*, **202**(11), pp. 2344–2348.
- [47] Voevodin, A. ., and Zabinski, J. ., 2000, "Supertough wear-resistant coatings with 'chameleon' surface adaptation," *Thin Solid Films*, **370**(1-2), pp. 223–231.
- [48] Voevodin, A. A., O'Neill, J. P., and Zabinski, J. S., 1999, "Nanocomposite tribological coatings for aerospace applications," *Surf. Coatings Technol.*, **116-119**, pp. 36–45.
- [49] Wu, J.-H., Sanghavi, M., Sanders, J. ., Voevodin, A. ., Zabinski, J. ., and Rigney, D. ., 2003, "Sliding behavior of multifunctional composite coatings based on diamond-like carbon," *Wear*, **255**(7-12), pp. 859–868.
- [50] Wu, J.-H., Rigney, D. A., Falk, M. L., Sanders, J. H., Voevodin, A. A., and Zabinski, J. S., 2004, "Tribological behavior of WC/DLC/WS₂ nanocomposite coatings," *Surf. Coatings Technol.*, **188-189**, pp. 605–611.
- [51] Nossa, A., and Cavaleiro, A., 2004, "Chemical and physical characterization of C(N)-doped W–S sputtered films," *J. Mater. Res.*, **19**(08), pp. 2356–2365.
- [52] Evaristo, M., Nossa, A., and Cavaleiro, A., 2005, "W–S–C sputtered films: Influence of the carbon alloying method on the mechanical properties," *Surf. Coatings Technol.*, **200**(1-4), pp. 1076–1079.
- [53] Nossa, A., and Cavaleiro, A., 2001, "The influence of the addition of C and N on the wear behaviour of W–S–C/N coatings," *Surf. Coatings Technol.*, **142-144**, pp. 984–991.

- [54] Nossa, a, and Cavaleiro, a, 2001, "The influence of the addition of C and N on the wear behaviour of W . S . CrN coatings," *Surf. Coatings Technol.*, pp. 984–991.
- [55] Nossa, a., and Cavaleiro, a., 2003, "Mechanical behaviour of W-S-N and W-S-C sputtered coatings deposited with a Ti interlayer," *Surf. Coatings Technol.*, **163-164**, pp. 552–560.
- [56] T. Polcar, F. Gustavsson, T. Thersleff, S. Jacobson, A. Cavaleiro, 2012, "Complex frictional analysis of self-lubricant W-S-C/Cr coating," *Faraday Discuss.*, **156**, pp. 383–401.
- [57] Noshiro, J., Watanabe, S., Sakurai, T., and Miyake, S., 2006, "Friction properties of co-sputtered sulfide/DLC solid lubricating films," *Surf. Coatings Technol.*, **200**(20-21), pp. 5849–5854.
- [58] Moser, J., and Lèvy, F., 1993, "MoS₂-x lubricating films: structure and wear mechanisms investigated by cross-sectional transmission electron microscopy," *Thin Solid Films*, **228**(1-2), pp. 257–260.
- [59] Singer, I. L., Fayeulle, S., and Ehni, P. D., 1996, "Wear behavior of triode-sputtered MoS₂ coatings in dry sliding contact with steel and ceramics," *Wear*, **195**(1-2), pp. 7–20.
- [60] Spalvins, T., 1982, "Morphological and frictional behavior of sputtered MoS₂ films," *Thin Solid Films*, **96**(1), pp. 17–24.
- [61] John, P. J., Prasad, S. V., Voevodin, A. A., and Zabinski, J. S., 1998, "Calcium sulfate as a high temperature solid lubricant," *Wear*, **219**(2), pp. 155–161.
- [62] Zabinski, J. S., Florkey, J. E., Walck, S. D., Bultman, J. E., and McDevitt, N. T., 1995, "Friction properties of WS₂/graphite fluoride thin films grown by pulsed laser deposition," *Surf. Coatings Technol.*, **76-77**, pp. 400–406.
- [63] Voevodin, A. A., O'Neill, J. P., and Zabinski, J. S., 1999, "WC/DLC/WS₂ nanocomposite coatings for aerospace tribology," *Tribol. Lett.*, **6**(2), pp. 75–78.
- [64] Rai, A. K., Bhattacharya, R. S., Zabinski, J. S., and Miyoshi, K., 1997, "A comparison of the wear life of as-deposited and ion-irradiated WS₂ coatings," *Surf. Coatings Technol.*, **92**(1-2), pp. 120–128.
- [65] Hirano, M., and Miyake, S., 1985, "Sliding life enhancement of a WS₂ sputtered film by ion beam mixing," *Appl. Phys. Lett.*, **47**(7).
- [66] Prasad, S. V., and Zabinski, J. S., 1993, "Tribology of tungsten disulphide (WS₂): characterisation of wear-induced transfer films," *J. Mater. Sci. Lett.*, **12**, pp. 1413–1415.

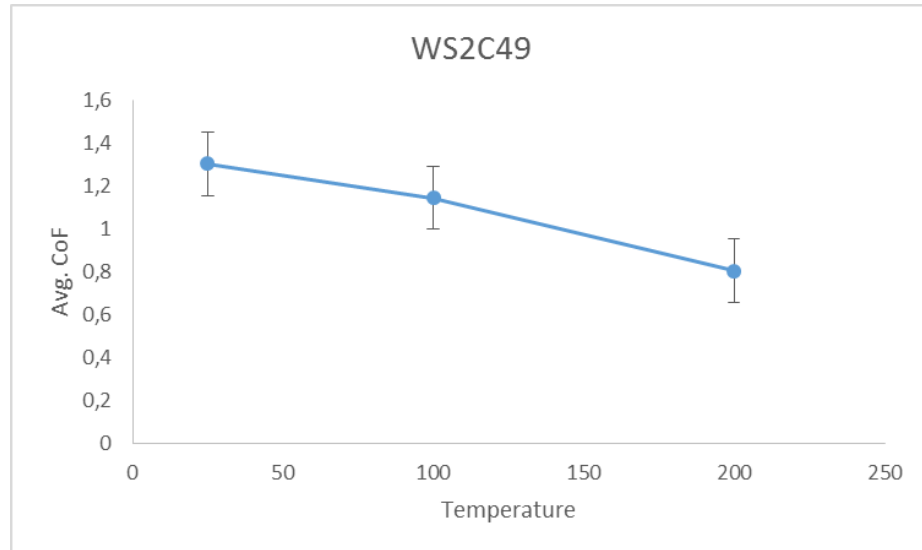
- [67] Waghray, H., Lee, T.-S., and Tatarchuk, B. J., 1995, "A study of the tribological and electrical properties of sputtered and burnished transition metal dichalcogenide films," *Surf. Coatings Technol.*, **76-77**, pp. 415–420.
- [68] Koch, T., Evaristo, M., Pauschitz, a., Roy, M., and Cavaleiro, a., 2009, "Nanoindentation and nanoscratch behaviour of reactive sputtered deposited W-S-C film," *Thin Solid Films*, **518**(1), pp. 185–193.
- [69] Doraiswamy, N., and Marks, L. D., 1995, "Ultrahigh-Vacuum High-Resolution Transmission Electron Microscopy of Sputter-Deposited MoS₂ Thin Films," **94**(4935).
- [70] Callisti, M., and Polcar, T., 2014, "The role of Ni–Ti–(Cu) interlayers on the mechanical properties and nano-scratch behaviour of solid lubricant W–S–C coatings," *Surf. Coatings Technol.*, **254**, pp. 260–269.
- [71] Polcar, T., Evaristo, M., Stueber, M., and Cavaleiro, A., 2009, "Mechanical and tribological properties of sputtered Mo–Se–C coatings," *Wear*, **266**(3-4), pp. 393–397.
- [72] Polcar, T., Evaristo, M., and Cavaleiro, A., 2007, "Friction of self-lubricating W-S-C sputtered coatings sliding under increasing load," *Plasma Process. Polym.*, **4**(SUPPL.1), pp. 541–546.
- [73] Polcar, T., Evaristo, M., and Cavaleiro, A., 2009, "Self-lubricating W-S-C nanocomposite coatings," *Plasma Process. Polym.*, **6**(6-7), pp. 417–424.
- [74] Polcar, T., Evaristo, M., Colaço, R., Silviu Sandu, C., and Cavaleiro, A., 2008, "Nanoscale triboactivity: The response of Mo–Se–C coatings to sliding," *Acta Mater.*, **56**(18), pp. 5101–5111.
- [75] Moore, D. F., 1972, *The friction and lubrication of elastomers*, Pergamon Press.
- [76] Pearson, B. N. ., 1998, "On the theory of rubber friction," *Surf. Sci.*, **401**, pp. 445–454.
- [77] Delor, F., Lacoste, J., Lemaire, J., Barrois-Oudin, N., and Cardinet, C., 1996, "Photo- and thermal ageing polychloroprene: effect of carbon black and crosslinking," *Polym. Degrad. Stabil.*, **53**(361).
- [78] Grassie, N., and Heaney, A., 1974, "Thermal degradation of copolymers of butadiene and acrylonitrile," *Eur. Polym. J.*, **15**(10), pp. 415–424.
- [79] Shanghai Stal Precision Stainless Steel Co. LTD, 2013, "Types 316 (S31600), 316L (S31603), 317 (S31700), 317L (S31703)," **316**.
- [80] Moser, J., and Lévy, F., 1994, "Random stacking in MoS_{2-x} sputtered thin films," *Thin Solid Films*, **240**(1-2), pp. 56–59.

- [81] Polcar, T., Evaristo, M., and Cavaleiro, A., 2007, “The tribological behavior of W–S–C films in pin-on-disk testing at elevated temperature,” *Vacuum*, **81**(11-12), pp. 1439–1442.
- [82] Evaristo, M., Nossa, a, and Cavaleiro, a, 2006, “Tribological Behaviour of Reactive and Co-Sputtered W-S-C Coatings,” **18**.
- [83] Polcar, T., and Cavaleiro, A., 2011, “Self-adaptive low friction coatings based on transition metal dichalcogenides,” *Thin Solid Films*, **519**(12), pp. 4037–4044.

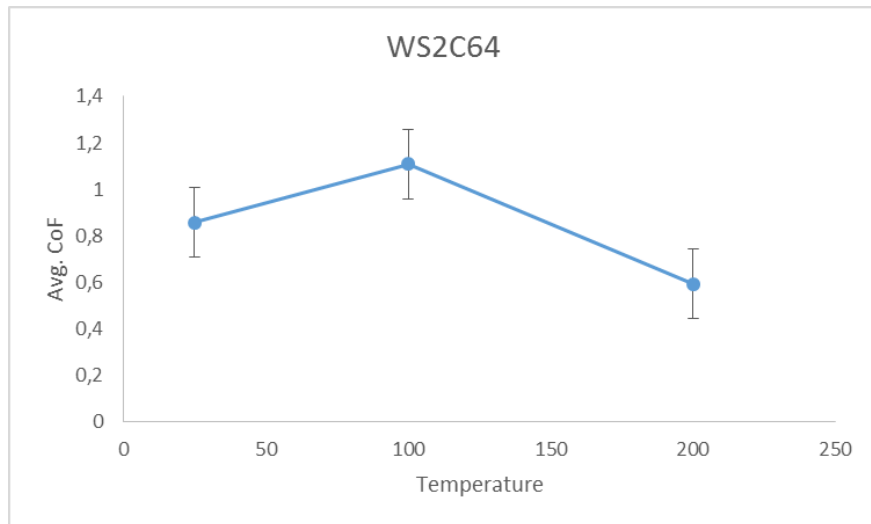
7. Appendix



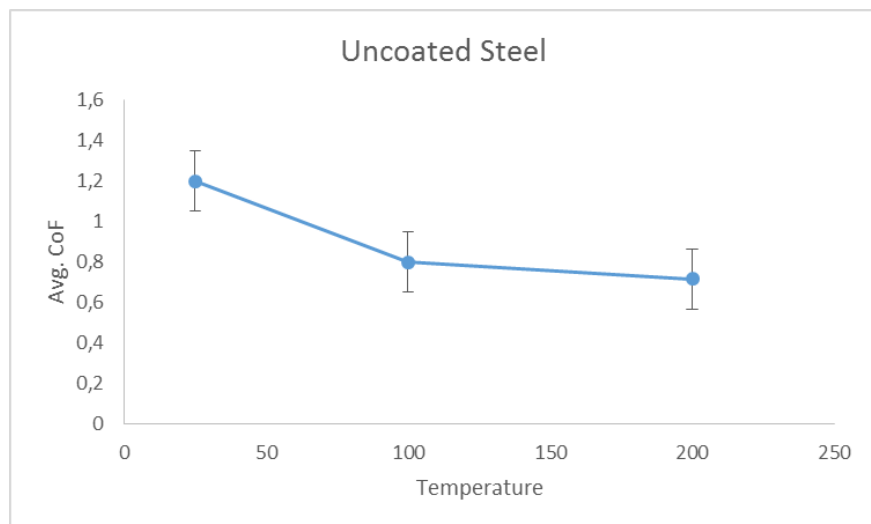
Appendix Fig 1 - CoF variation of pure W-S vs temperature



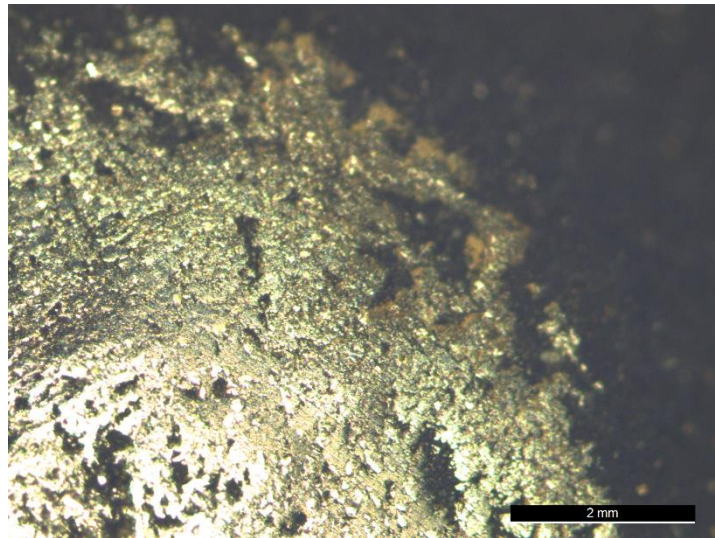
Appendix Fig 2 - CoF variation of WSC49 vs temperature



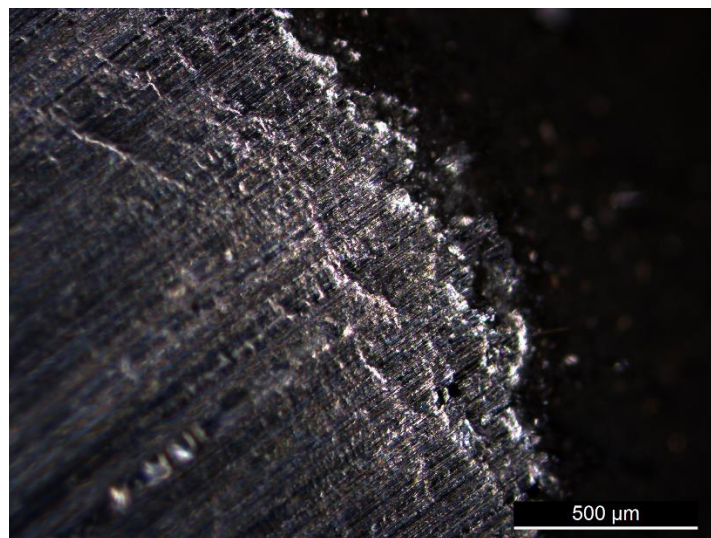
Appendix Fig 3 - CoF variation of WSC64 vs temperature



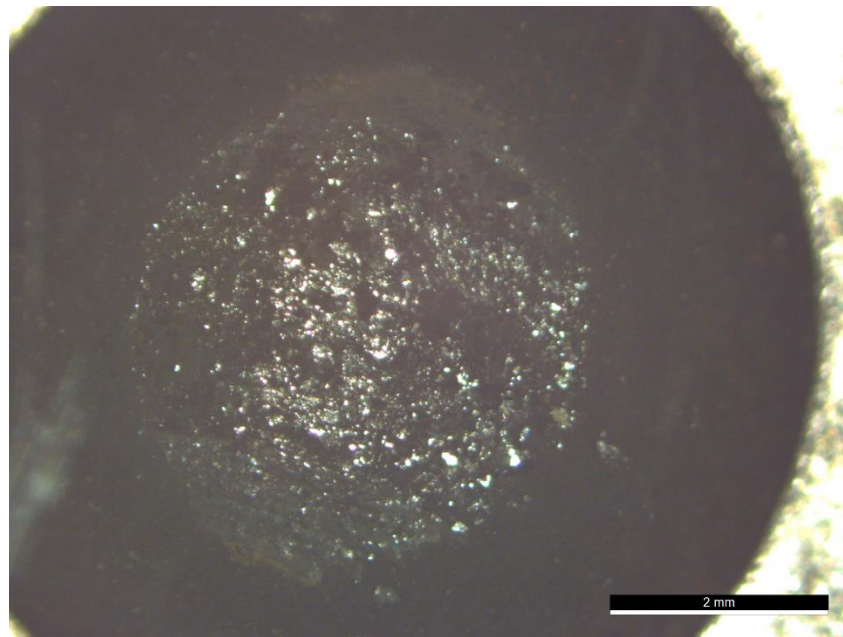
Appendix Fig 5 - CoF variation of WSC64 vs temperature



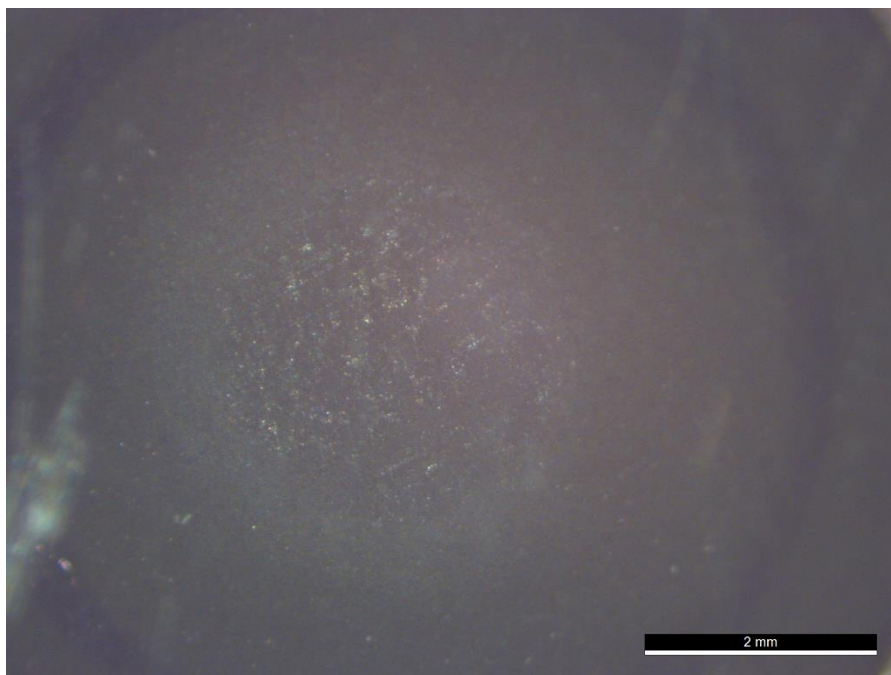
Appendix Fig 6 – *Optical image of NBR surface after test against uncoated steel at 200 °C (5000 cycles)*



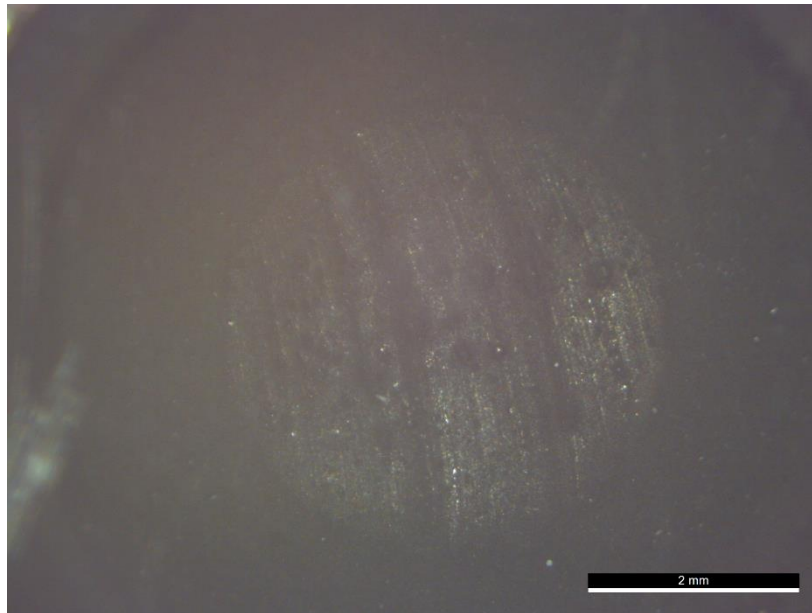
Appendix Fig 7 – *Optical image of NBR surface after test against pure W-S coating at 200 °C (5000 cycles)*



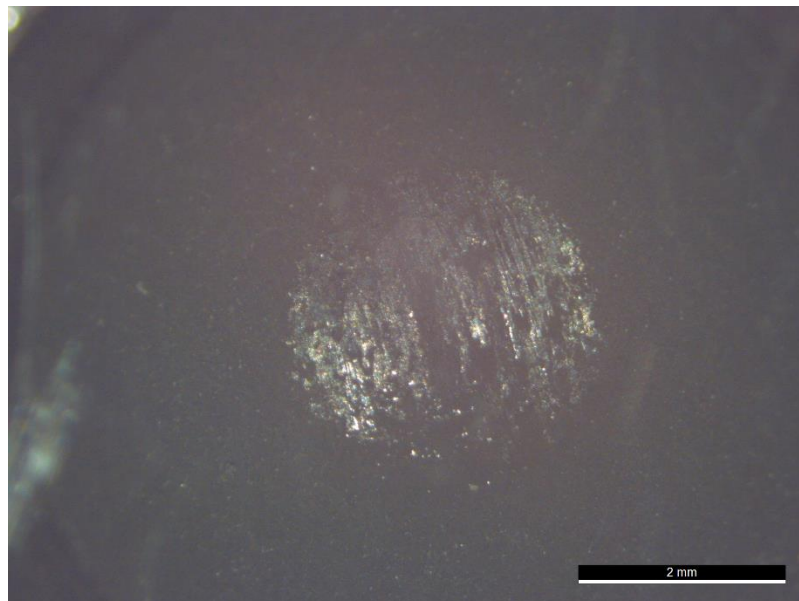
Appendix Fig 8 – *Optical image of NBR surface after test against uncoated steel at RT (60000 cycles)*



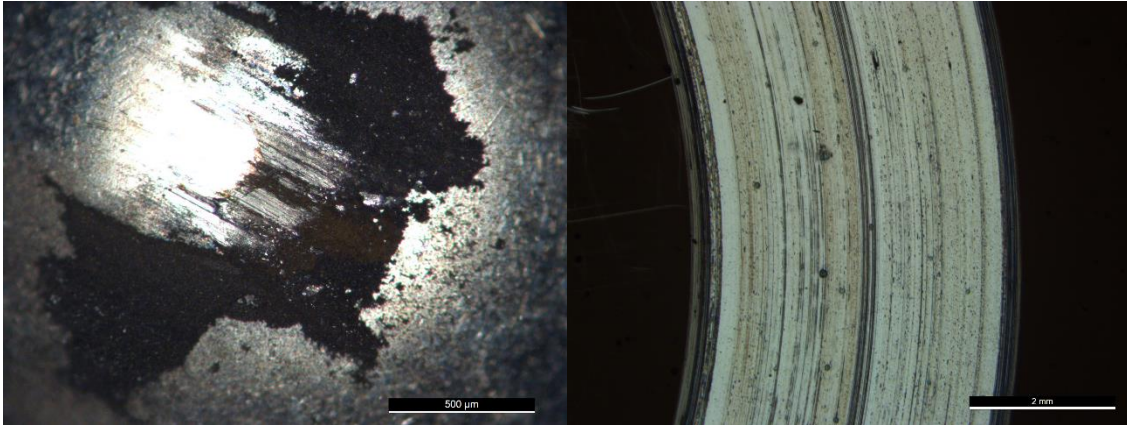
Appendix Fig 9 – *Optical image of NBR surface after test against pure W-S coating at RT (60000 cycles) (after removal of wear debris)*



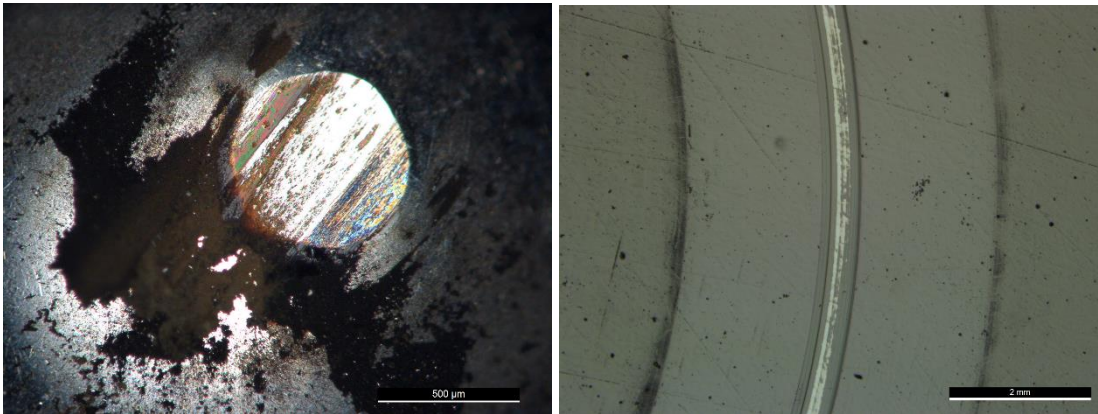
Appendix Fig 10 – *Optical image of NBR surface after test against WSC49 coating at 100 °C (5000 cycles) (after removal of wear debris)*



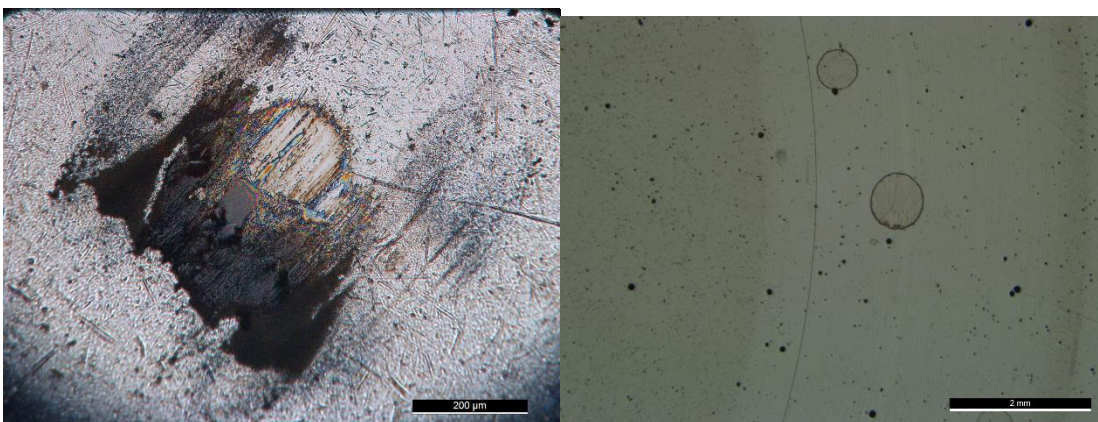
Appendix Fig 11 – *Optical image of NBR surface after test against WSC49 coating at 200 °C (5000 cycles) (after removal of wear debris)*



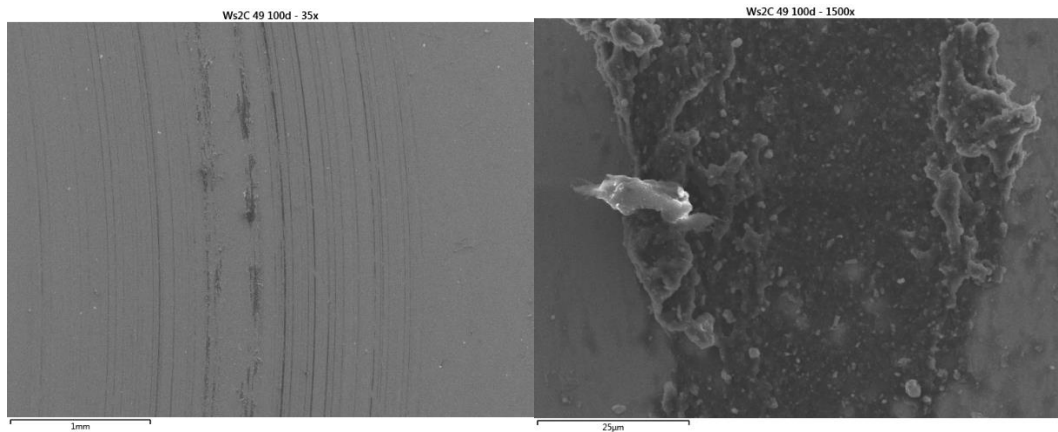
Appendix Fig 12 – Optical image of 100Cr6 surface (left) after test against pure W-S coating at RT (2000 cycles) and the subsequent wear track (right) after the use of NBR (60000 cycles)



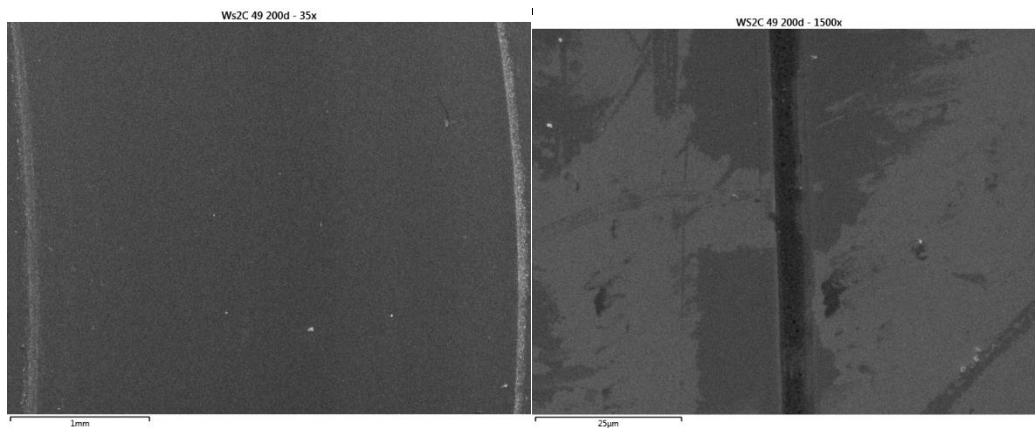
Appendix Fig 13 – Optical image of 100Cr6 surface (left) after test against WSC64 coating at RT (2000 cycles) and the subsequent wear track (right) after the use of NBR (60000 cycles)



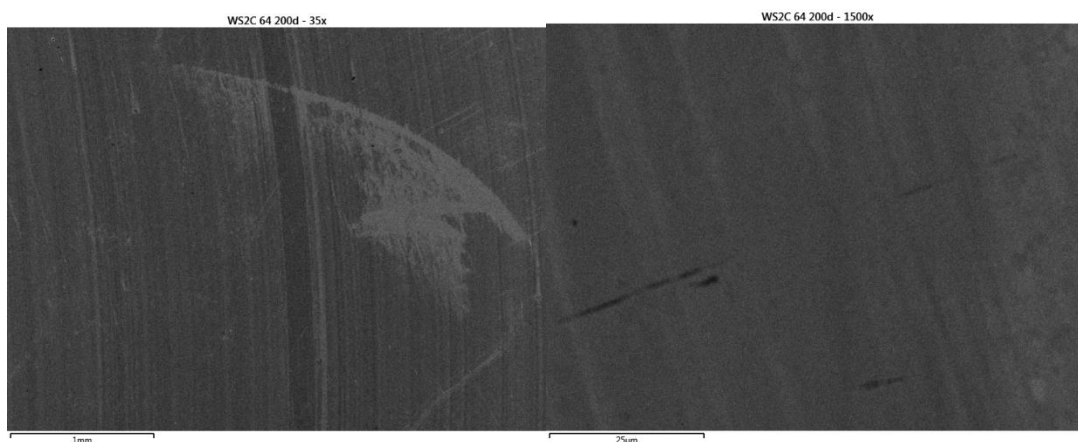
Appendix Fig 14 – Optical image of 100Cr6 surface (left) after test against WSC49 coating at RT (2000 cycles) and the subsequent wear track (right) after the use of NBR (60000 cycles)



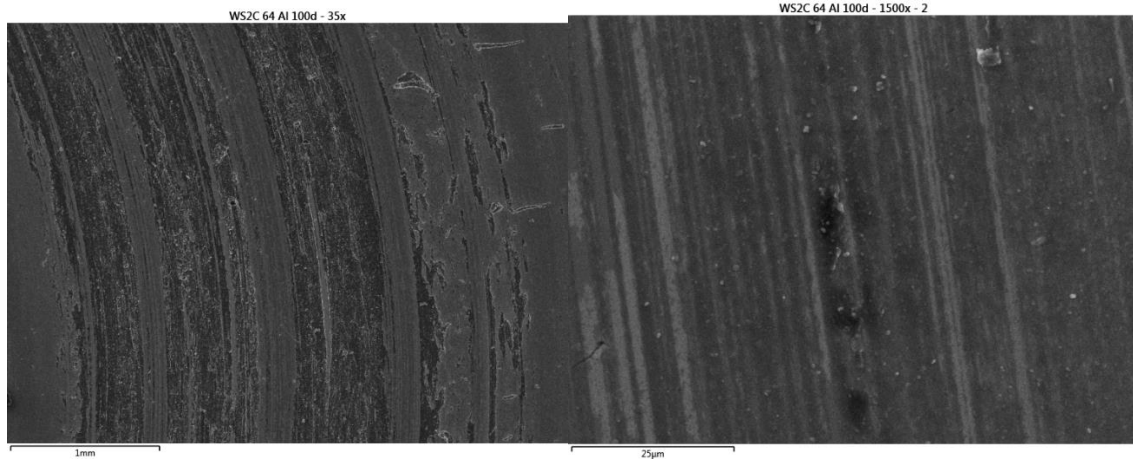
Appendix Fig 15 – SEM images of WSC49 surface wear track at 35x magnification (left) and at 1500x magnification (right) after the use of NBR (5000 cycles) at 100 °C.



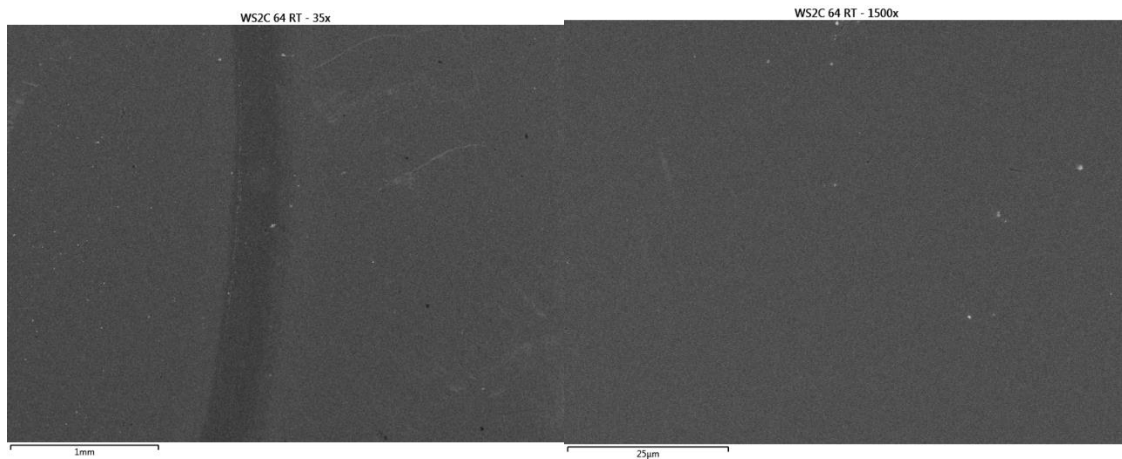
Appendix Fig 16 – SEM images of WSC49 surface wear track at 35x magnification (left) and at 1500x magnification (right) after the use of NBR (60000 cycles) at 200 °C.



Appendix Fig 17 – SEM images of WSC64 surface wear track at 35x magnification (left) and at 1500x magnification (right) after the use of NBR (60000 cycles) at 200 °C.



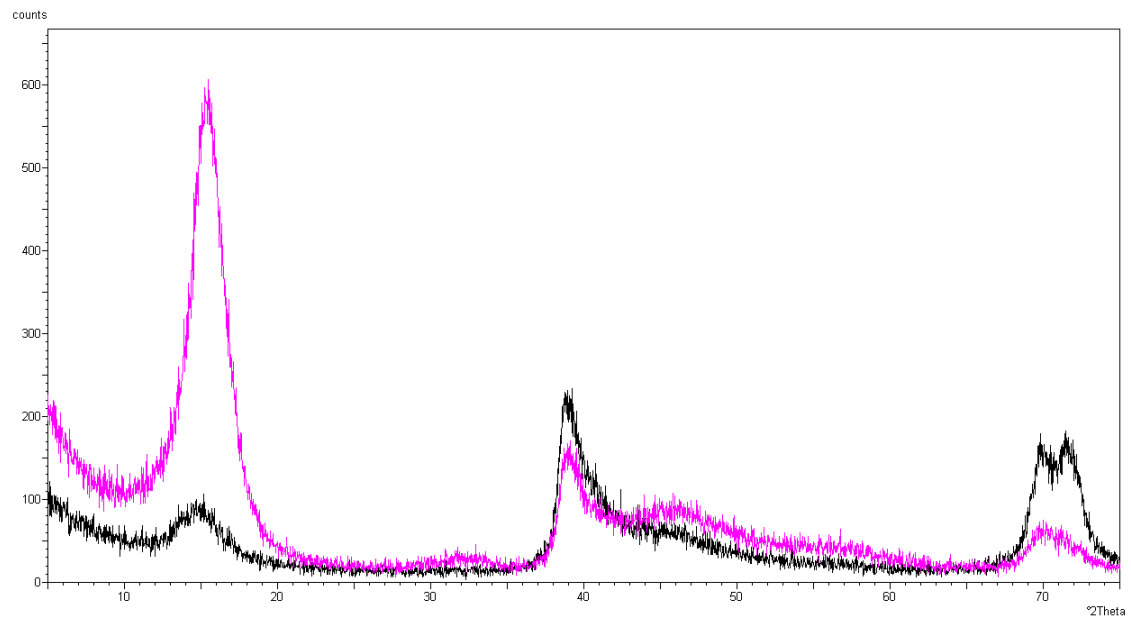
Appendix Fig 18 – SEM images of WSC64 surface wear track at 35x magnification (left) and at 1500x magnification (right) after the use of NBR (5000 cycles) at 100 °C.



Appendix Fig 19 – SEM images of WSC64 surface wear track at 35x magnification (left) and at 1500x magnification (right) after the use of NBR (60000 cycles) at RT.

	C	O	S	Ca	W	Total
WSC49 (100C)	82,5	13,01		3,45	1,04	100
WSC49 (200C) LC	73,96	15,95	3,99		6,10	100
WSC64 (200C) LC	69,84		17,27		12,90	100
WSC64 (100C)	82,02	14,22		3,75		100
WSC64 (RT)	65,86		19,89		14,26	100

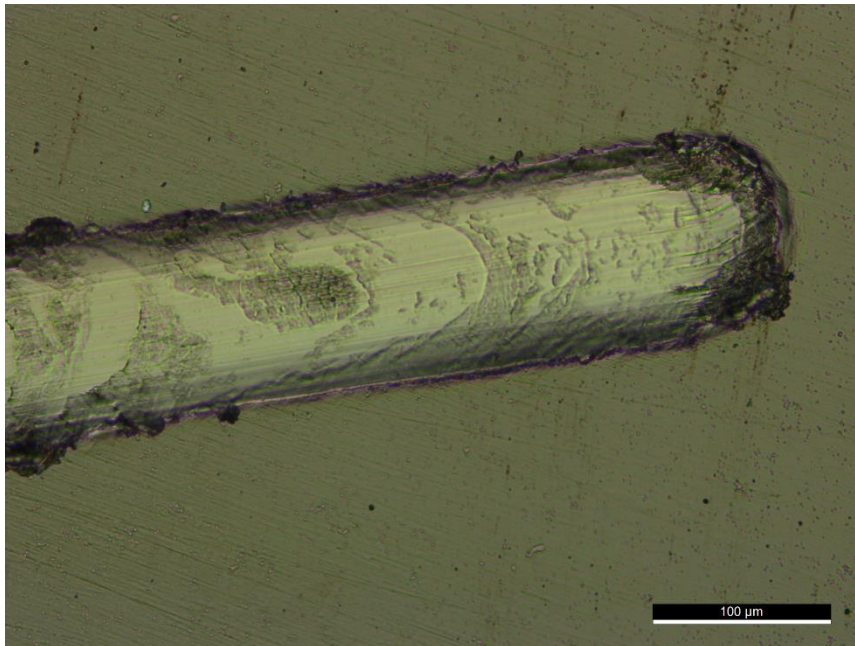
Appendix (Table) 20 – Table summarizing the analysis results of the composition of the wear tracks studied using EDS



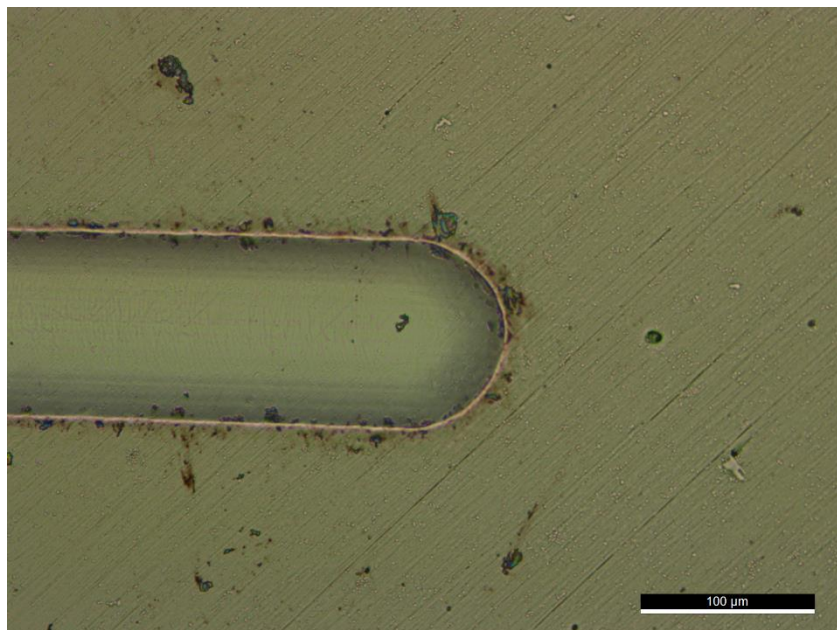
Appendix Fig 21 – Comparison XRD spectra for pure W-S coating (as deposited) in black and pure W-S coating (after rubbing with cotton) in pink. Characteristic 10L peak occurs at $2\theta \approx 40^\circ$ in both the cases.



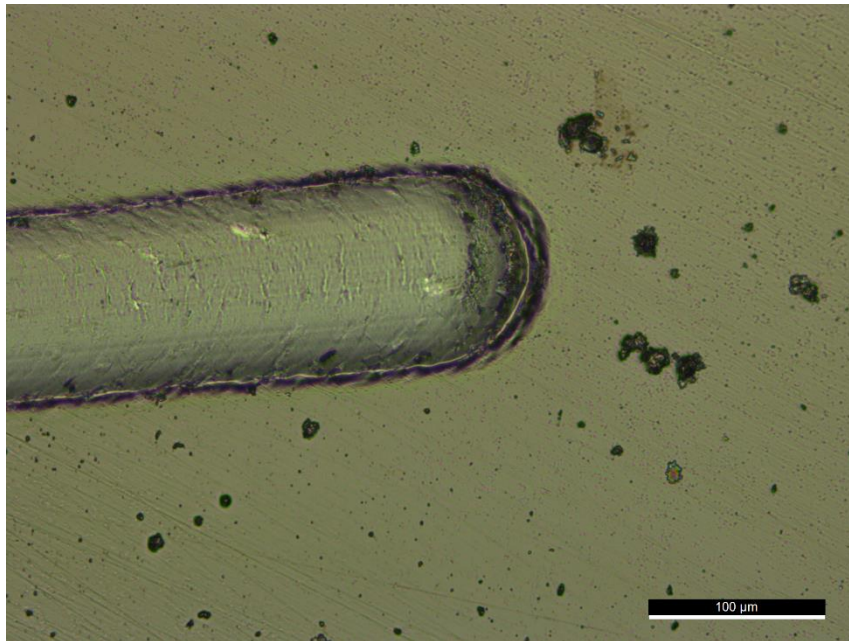
Appendix Fig 22 – Image of the adhesion test results on WSC49 (centre deposited) coating. The critical load was greater than 50 mN



Appendix Fig 23 – Image of the adhesion test results on WSC49 (periphery deposited) coating. The coating delaminates at a critical load lower than 50 mN.



Appendix Fig 24 – Image of the adhesion test results on WSC64 (center deposited) coating. The coating has a critical load higher than 50 mN.



Appendix Fig 25 – Image of the adhesion test results on WSC64 (periphery deposited) coating. The coating almost delaminates at a critical load lower than 50 mN.